p. 61

DEVELOPMENT OF A FRESNEL LENS

GALLIUM ARSENIDE PHOTOVOLTAIC

CONCENTRATOR FOR SPACE APPLICATIONS

SBIR 1985 Phase II

BY

M. J. O'NEILL
A. J. McDANAL
J. L. PERRY

ENTECH, INC.
1015 ROYAL LANE
P.O. BOX 612246
DFW AIRPORT, TX 75261

PHONE: 214-456-0900
TELEFAX: 214-456-0904

OCTOBER 1990

FINAL REPORT

SBIR - 10-08-0900

RELEASE DATE 10-8-92

ENTECH, INC.

Development of a Fresnel Lens Gallium Arsenide

Photovoltaic Concentrator for Space Applications

(Final Report for NASA SBIR Phase II Contract No. NAS3-25192)

CONTENTS

Acknowledgements

1.0 Summary

In 1986, under a Phase I SBIR project, ENTECH generated a conceptual design for a new space photovoltaic power system. The proposed new system would utilize a matrix of transmittance-optimized mini-dome Fresnel lenses to focus sunlight onto a corresponding matrix of prism-covered gallium arsenide cells, using a lightweight aluminum honeycomb/radiator structure to support the lenses and cells. The predicted efficiency levels were unprecedented:

1. Mini-dome lenses should achieve over 90% net optical efficiency at 109X geometric concentration ratio, and should tolerate sun-tracking errors of up to 1 degree without loss in performance.

2. Prism-covered gallium arsenide cells should achieve 24% efficiency at 25C, and 22% at 100C, under 100 AMO suns irradiance.

3. With such excellent optical and electrical performance levels, the new system should provide nearly 240 W/sq.m. of areal power density.

4. Including the aluminum honeycomb/radiator panel structure plus an automatically deploying multi-panel array support structure, the new system should have a mass/area ratio of only 3.2 kg/sq.m. (which is about the same as for the one-sun silicon cell Kapton blanket array being developed for the Space Station Freedom). With this low mass, the new system should provide about 75 W/kg of specific power.

The primary objective of this Phase II SBIR project was to develop and test prototype hardware to verify these theoretically predicted performance levels. Over the past three years, we have successfully developed the new lens, the new prism-covered gallium arsenide cell, and the aluminum radiator/honeycomb panel structure. High-altitude airplane flight tests by NASA Lewis have confirmed 90% net optical efficiency for the new lens. Outdoor tests by ENTECH have also confirmed the tracking error tolerance of the new lens.

Solar simulator tests by NASA Lewis have confirmed 24% cell efficiency at 25C and 22% cell efficiency at 100C, after prismatic covers were applied to the gallium arsenide cells. Furthermore, Boeing has recently developed a low-bandgap gallium antimonide cell which can be placed behind an infrared-transparent, high-bandgap gallium arsenide cell in a mechanically stacked tandem cell assembly. With prismatic covers on both cells, NASA Lewis airplane flight tests, coupled with solar simulator tests, have confirmed about 31% AMO efficiency at 25C for the tandem cell assembly.

In support of our program, Boeing has fabricated several honeycomb/radiator panel structures, using a rapid, low-cost, computer-controlled milling process to machine the panel out of a thick plate of aluminum. This method provides unequaled design flexibility, in addition to outstanding structural and thermal performance. A thirty-six element prototype panel, populated with cells and lenses, was fabricated, tested, and delivered to NASA Lewis under this program. This prototype panel successfully demonstrated the simplicity and practicality of the mini-dome lens panel concept.

Based on the results of this project, we are confident that the mini-dome lens concentrator system can achieve over 300 W/sq.m. of areal power density and over 100 W/kg of specific power in the near term, using the tandem cell technology.
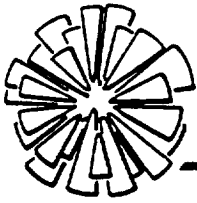
2.0 Introduction and System Description

In 1986, under a Phase I NASA Small Business Innovation Research (SBIR) contract, we performed a thorough analytical evaluation of the technical feasibility of adapting our terrestrial Fresnel lens photovoltaic concentrator technology to space applications (Reference 1). Under the Phase I study, we analyzed a variety of candidate optical concentrator approaches, including linear Fresnel lenses which provide a line focus, crossed linear Fresnel lenses which produce a point focus, and dome-shaped Fresnel lenses which produce a point focus. The transmittance-optimized mini-dome lens concentrator was selected, because it should simultaneously provide excellent optical efficiency (> 90%), excellent tracking error tolerance (>1 degree), high solar flux concentration (> 100 suns), and unequaled shape error tolerance (100 times better than flat lenses or reflective concentrators). Our unique lens, which can be configured in either a line-focus or point-focus embodiment, has been thoroughly described in previous publications (References 2, 3, and 4), and is the key element in ENTECH's terrestrial photovoltaic concentrator systems (References 5, 6, and 7).

Under the Phase I study, we likewise considered a variety of candidate solar cell approaches. After much analysis, we selected a gallium arsenide cell equipped with our performance-boosting prismatic cover, which effectively eliminates the normal gridline obscuration loss (References 8, 9, and 10). Gallium arsenide was selected over silicon because of its higher initial efficiency, its slower degradation rate under particulate radiation exposure in orbit, and its milder temperature coefficient. Trade studies were also conducted to define the best combination of irradiance profile over the cell, gridline pattern on the cell, and sun-tracking error tolerance. We predicted a prism-covered cell efficiency of 24% at 25C and 100 AMO suns irradiance for the selected cell design.

Under the Phase I study, we also evaluated several candidate approaches for the lens/cell panel support structure. We selected an aluminum radiator/honeycomb panel structure, which provides efficient waste heat rejection, excellent aperture area/panel area packing factor, exceptional stiffness/weight ratio, and very low cost potential. We predicted that the cell orbital operating temperature would be about 100C, with a 200 micron thick radiator, and that the resultant operating cell efficiency would be about 22%.
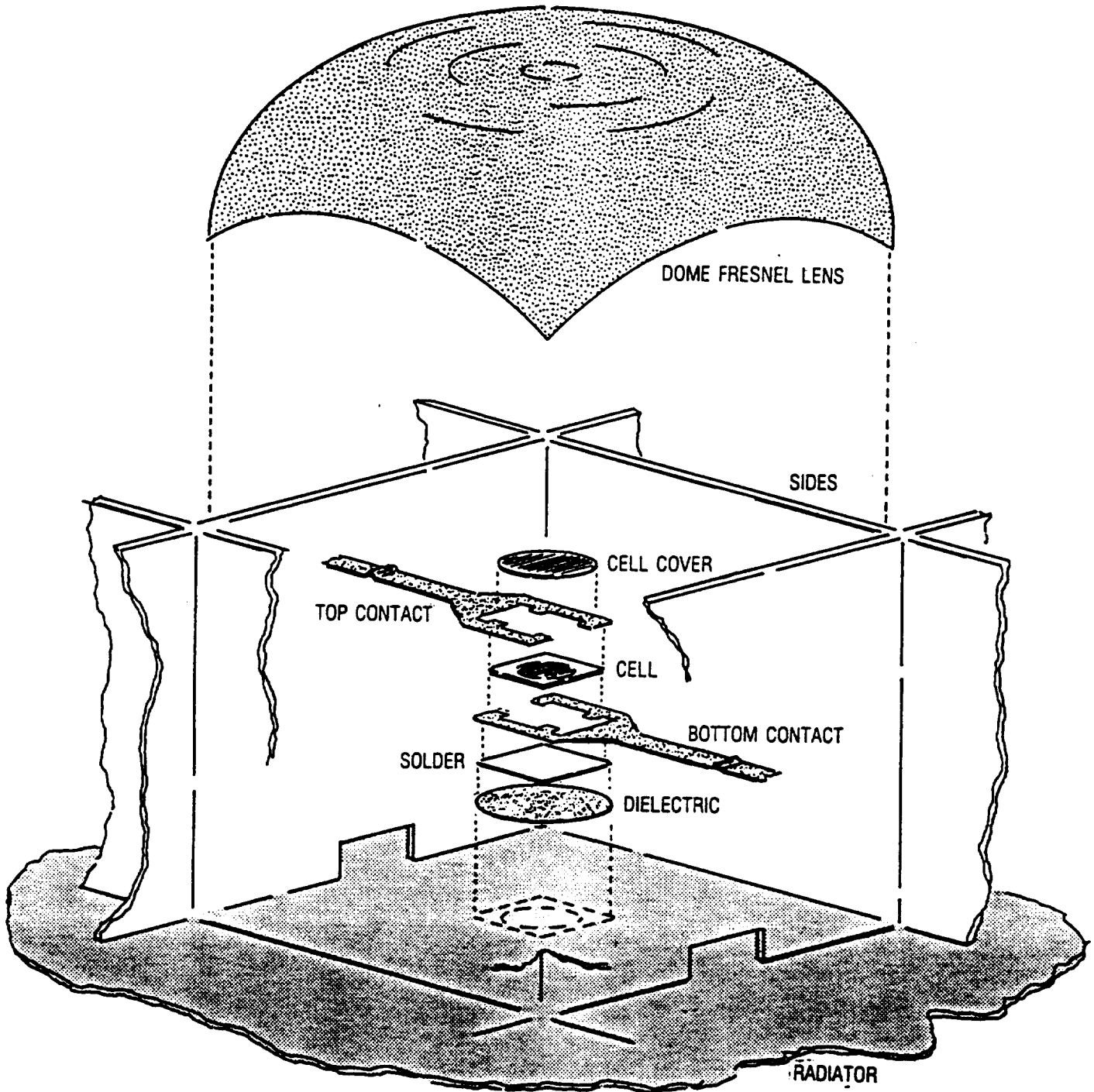
Figures 1, 2, and 3 show schematics of the mini-dome lens panel approach. The thin mini-dome Fresnel lens is trimmed to provide a square aperture and to fit into the square cavity corresponding to one element of the honeycomb panel structure. A prism-covered cell is mounted to the backplane radiator, which is located at the focal plane of the mini-dome lens. Each lens/cell combination is a separate functional module (Figure 1), with a power output of about one-third watt. Numerous modules are integrated together to form a panel (Figure 2), with a power output in the range of tens of watts, depending on size. The cells in a panel can be wired into parallel/series arrangements to provide any desired voltage/current output (Figure 3). The lenses can be recessed into the honeycomb structure to allow panels to be closely stacked without lens damage for launch and stowage (Figure 3). Lens, cell, and panel dimensions were selected primarily to be compatible with 100-sun, 4 mm diameter, gallium arsenide cells being developed under other NASA and DOD programs. Secondary considerations included panel thickness, tracking error tolerance, and radiator thermal performance. The resultant lens dimensions included a 3.7 cm by 3.7 cm aperture, a 4 cm focal length, and a corner ray turning angle of 51 degrees. The resultant panel mass was estimated to be about 2.5 kg/sq.m. of area.

Figure 1

DOME LENS PV MODULE CONCEPTUAL DESIGN

ENTECH, INC.

DOME FRESNEL LENS

SIDES

CELL COVER

TOP CONTACT

CELL

BOTTOM CONTACT

SOLDER

DIELECTRIC

RADIATOR
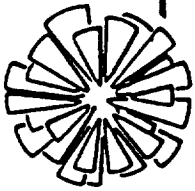
ENTECH DOME LENS PV CONCENTRATOR
PANEL CONCEPTUAL DESIGN

ENTECH, INC.

INCIDENT SUNLIGHT

REFRACTIVE DOME LENS

LENS SUPPORT

GaAs SOLAR CELL

RADIATOR

LENS/CELL MODULE

GALLIUM ARSENIDE CELL AND DIELECTRIC
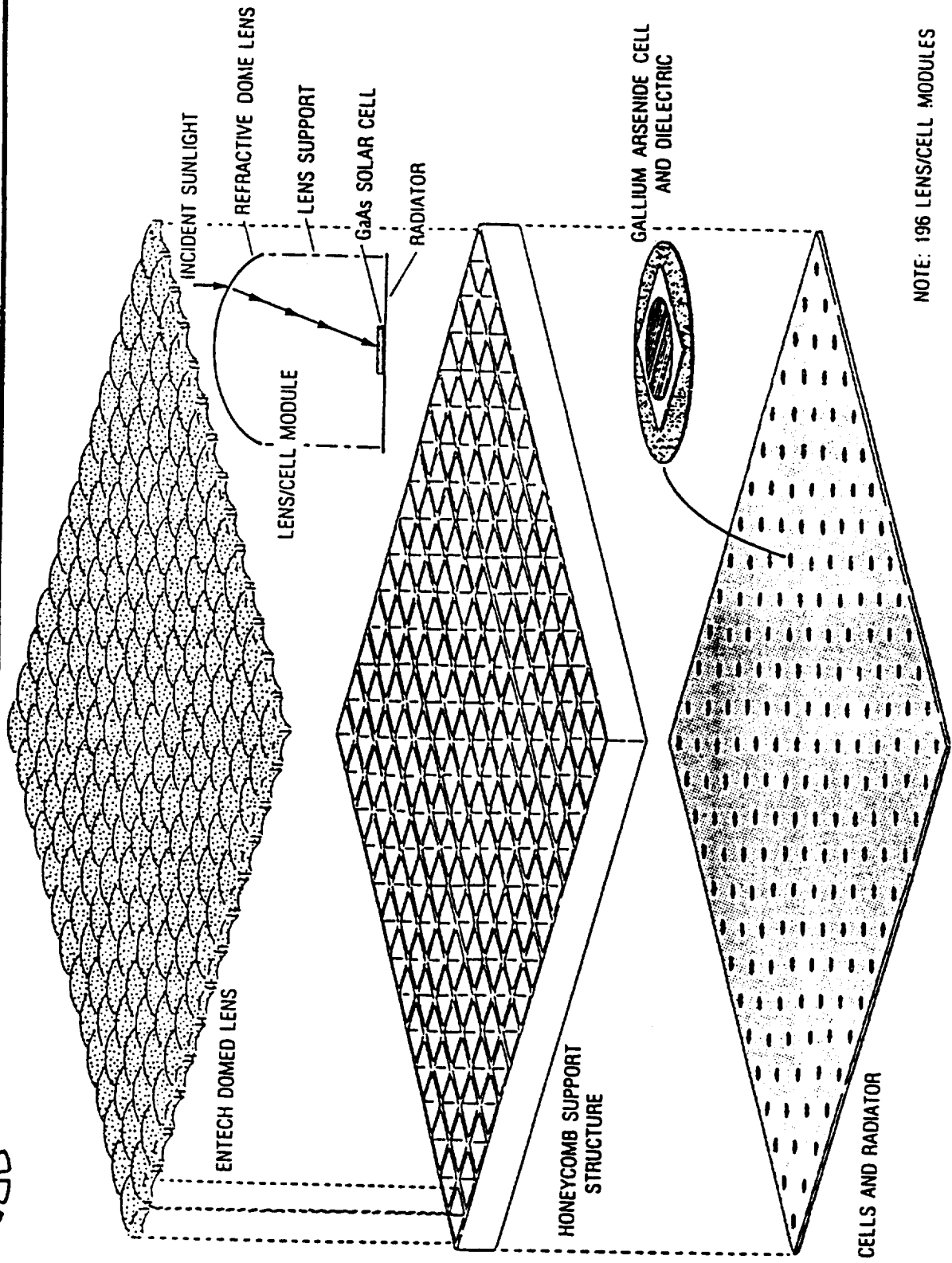
NOTE: 196 LENS/CELL MODULES

ENTECH DOMED LENS

HONEYCOMB SUPPORT STRUCTURE

CELLS AND RADIATOR

Figure 2

- 4 -
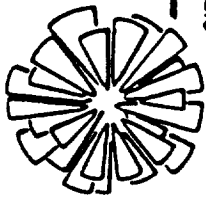
CROSS - SECTIONAL VIEWS OF DOME LENS PV PANEL

ENTECH, INC.

SIDE VIEW

4.05cm

$t_{honeycomb}$

$t_{radiator}$

SOLAR CELL

DOMED LENS

RADIATOR

TOP VIEW WITHOUT LENS

HONEYCOMB MATRIX

LENS EDGE RATAINER

GALLIUM ARSENIDE SOLAR CELL

ALUMINA SUBSTRATE

RADIATOR

3.75 cm

3.75 cm

Figure 3

- 5 -
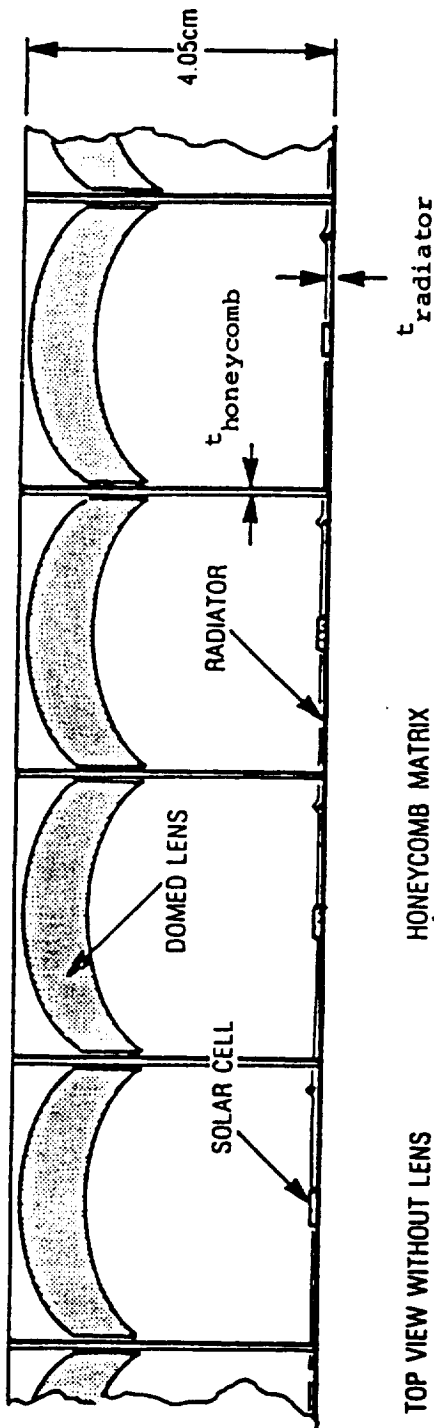
The mini-dome lens photovoltaic concentrator panel was also designed to be compatible with automatically deploying support structures being developed for NASA by other organizations. For example, Figure 4 shows the mini-dome lens panels integrated with Astro Aerospace Corporation's extendible support structure (ESS) attached to the Space Station (Reference 11). The ESS structure was designed for use with much heavier and less efficient reflective concentrators, and is thus over-designed for the mini-dome lens panel application. For example, Figure 4 shows the relative array sizes for equal power output of the dome lens concentrator (DLC) array versus the mini-Cassegrainian concentrator (MCC) array which is being developed by TRW. The mass of the ESS structure is very low, corresponding to about 0.7 kg/sq.m. of panel area.

Based on the predicted performance levels and mass estimates mentioned above, the key conclusion of the Phase I study was that the new mini-dome lens system should be capable of providing an areal power density of nearly 240 W/sq.m., and a specific power of 75 W/kg in the near term. Both of these values 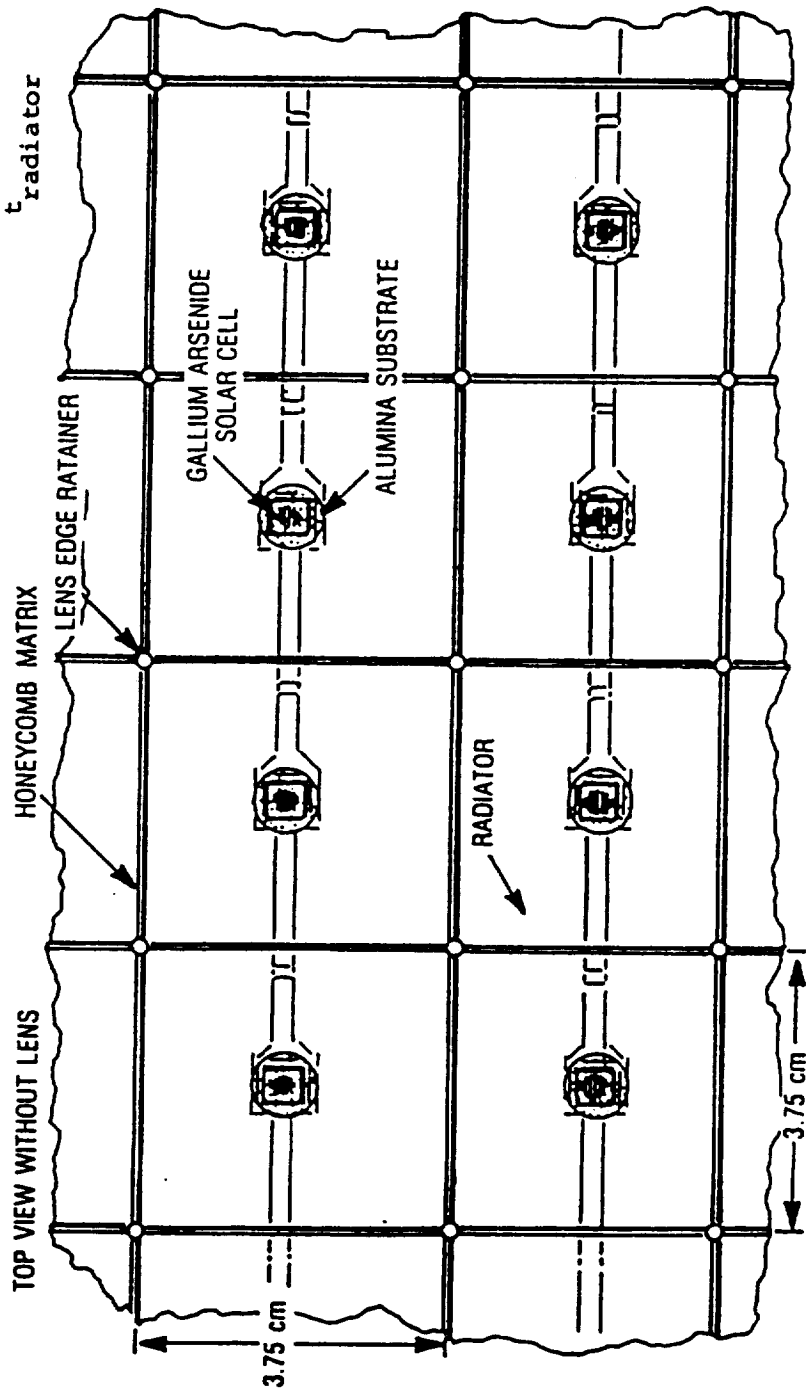represent at least a 50% improvement over state-of-the-art space photovoltaic power systems, including the one-sun silicon cell Kapton blanket array currently being developed for the Space Station Freedom.

In 1987, we were awarded a NASA Phase II SBIR contract to develop prototype hardware to verify these predicted performance levels. Over the past three years, with substantial assistance from NASA Lewis and from our industrial partners, we have successfully developed the new lens, the new prism-covered photovoltaic cell, and the honeycomb/radiator panel structure. Figure 5 shows a prototype mini-dome lens panel, which was developed, tested, and delivered under this program. As described in the following sections of this report, measured performance levels for prototype hardware have confirmed the Phase I predictions. Indeed, with recently developed tandem cell technology, we have now raised our near-term goals for the mini-dome lens photovoltaic concentrator system to 300 W/sq.m. of areal power density and 100 W/kg of specific power.

DOME LENS
PV ARRAYS ON ESS SYSTEM
ATTACHED TO SPACE STATION

ENTECH, INC.

0.4 m

2.74 m

STOWED CONFIGURATION

PARTIALLY DEPLOYED

DLC

MCC

2.1 m

3.5 m

6.3 m

DEPLOYED CONFIGURATION

SOURCE: NASA-CR-176394

Figure 4

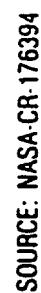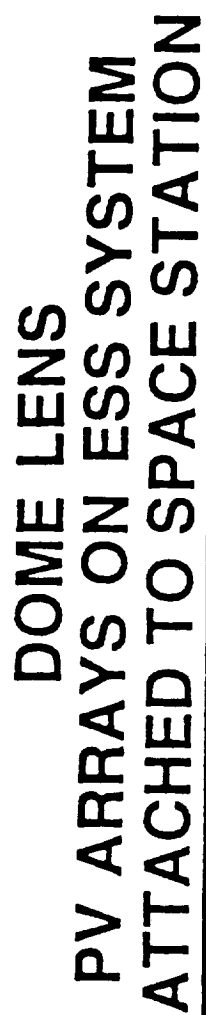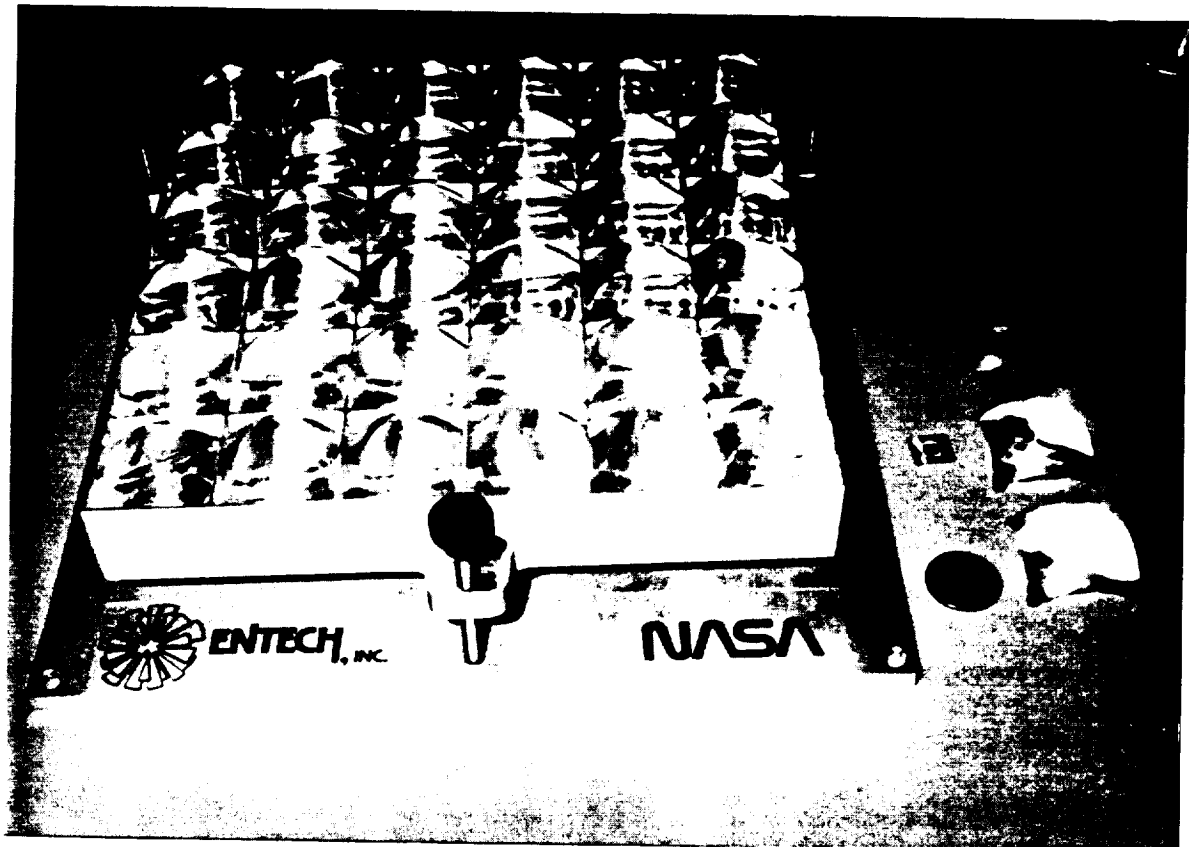- 7 -

Figure 5 - Prototype Mini-Dome Lens Photovoltaic Concentrator Panel

3.0 Mini-Dome Fresnel Lens Development

Figure 6 shows a schematic of the selected mini-dome Fresnel lens design. The lens is a laminated assembly comprising a ceria-doped microglass superstrate bonded to a clear silicone rubber (RTV) Fresnel lens substrate. Initial material investigations by ENTECH, NASA Lewis, and our industrial partners have identified the lens structure shown in Figure 6 as the best choice of materials for fabrication of the first concentrator lenses. The ceria-doped microglass provides protection for the silicone rubber lens against attack by monatomic oxygen (in low earth orbit); ultraviolet radiation; and particulate radiation. The silicone rubber prismatic pattern represents the functional optical element. Both the glass and the silicone rubber have been used for many years in space one-sun photovoltaic arrays. The microglass has been used as a cover slide material for one-sun silicon cells, while the silicone rubber has been used to bond the cover slides to the cells. This structure still must undergo extensive environmental testing. However, based on the history of these materials in space, we expect them to survive most space environmental conditions. (A monolithic lens made of a single material would have significant advantages over the present laminated lens structure, in terms of simplicity, manufacturability, weight, and cost. Research should continue on such a monolithic lens, especially for higher orbit applications, where mass is the most critical figure of merit, and where monatomic oxygen is no longer a factor.)

The 6 mil (150 micron) glass thickness has been selected to minimize handling losses; a thinner glass would provide adequate protection. The 8 mil (200 micron) total silicone rubber thickness corresponds to 4 mils of prismatic pattern and four mils of base thickness, including adhesive layer. The prism size was selected as a compromise between silicone mass and diffractive image spreading. The lens focal length is 4.0 cm. The lens has a square aperture 3.7 cm on a side, thereby providing about 13.7 sq.cm. of aperture area.

Figure 7 shows a cross-sectional schematic of the lens with greatly exaggerated prism size. Note that each prism in the lens is different in configuration. Figure 8 shows a magnified view of several prisms within the dome lens, including the sunlight passing through the lens. Note that the angle of incidence of the solar rays entering the outer smooth surface of the lens is equal to the angle of emergence of the rays leaving the inner faceted surface of the lens. This symmetrical refraction condition minimizes reflection losses, thereby providing the highest possible optical efficiency (References 2, 3, and 4). In addition, this symmetrical refraction condition minimizes image size and maximizes tolerance levels for manufacturing and operational inaccuracies. The lens is also configured to tolerate blunt tips on the prisms, which generally occur during a molding operation.

Although the previous paragraphs have described the basic lens configuration and geometry, the individual prism angles can be selected to provide virtually any desired focal plane irradiance profile over the photovoltaic cell. In consultation with NASA Lewis personnel, we selected a circular cell active area with a 4 mm diameter. In addition, we jointly selected 1 degree as the maximum anticipated sun-tracking error. A 1 degree sun-pointing error corresponds to an image displacement of 0.7 mm in the focal plane, due to the 4 cm focal length of the lens. Therefore, we selected the individual lens facet angles to spread out the concentrated solar irradiance over a 2.6 mm diameter target area at the middle of the 4.0 mm diameter active area. This allows for an image displacement in any direction of up to 0.7 mm, without spilling available photons beyond the
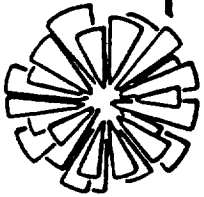
BASELINE LENS DESIGN FOR LOW-EARTH-ORBIT (LEO) APPLICATIONS
(MICROGLASS SHIELDS POLYMERIC LENS FROM ATOMIC OXYGEN)

LAMINATED CERIA MICROGLASS/SILICONE RTV MINI-DOME FRESNEL LENS

6 mil Thick Glass Dome

8 mil Thick Silicone RTV Prismatic Lens

3.7 cm

4 cm

Optical Axis
(Axis of Rotational Symmetry)

Focal Plane
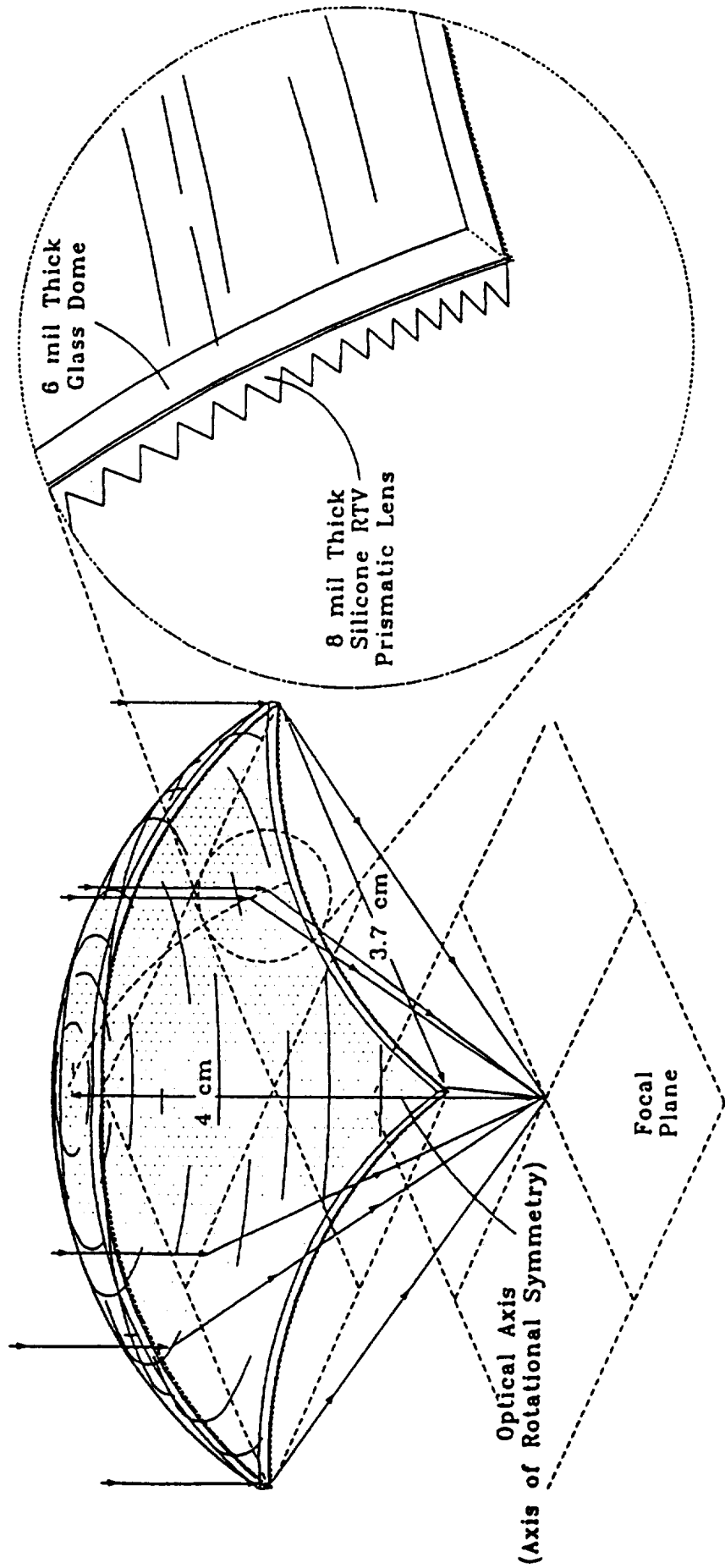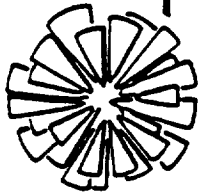
Figure 6

ENTECH, INC.

CROSS-SECTIONAL SCHEMATIC OF ENTECH'S PATENTED
SYMMETRICAL-REFRACTION LENS (U.S. PATENT 4,069,812)

Entech Mini-Dome Fresnel Lens Schematic and Nomenclature

Convex Outer Surface

Prism Size Greatly
Exaggerated for
Clarity

α

$\phi_{1/4}$

r_2 r_1

ϕ_2 Optical Axis (Axis of Rotational Symmetry)

ϕ_1

Focal Plane

Figure 7

MAGNIFIED VIEW OF SEVERAL PRISMS WITHIN
THE ENTECH DOME LENS, SHOWING REFRACTION
SYMMETRY AND BLUNT TIP TOLERANCE

THIS SYMMETRICAL REFRACTION CONDITION MINIMIZES REFLECTION LOSSES
FOR A GIVEN RAY TURNING ANGLE, THEREBY MAXIMIZING TRANSMITTANCE.

THE SYMMETRICAL REFRACTION CONDITION ALSO MINIMIZES IMAGE SIZE
AND MAXIMIZES TOLERANCE FOR MANUFACTURING ERRORS AND ABERRATIONS.
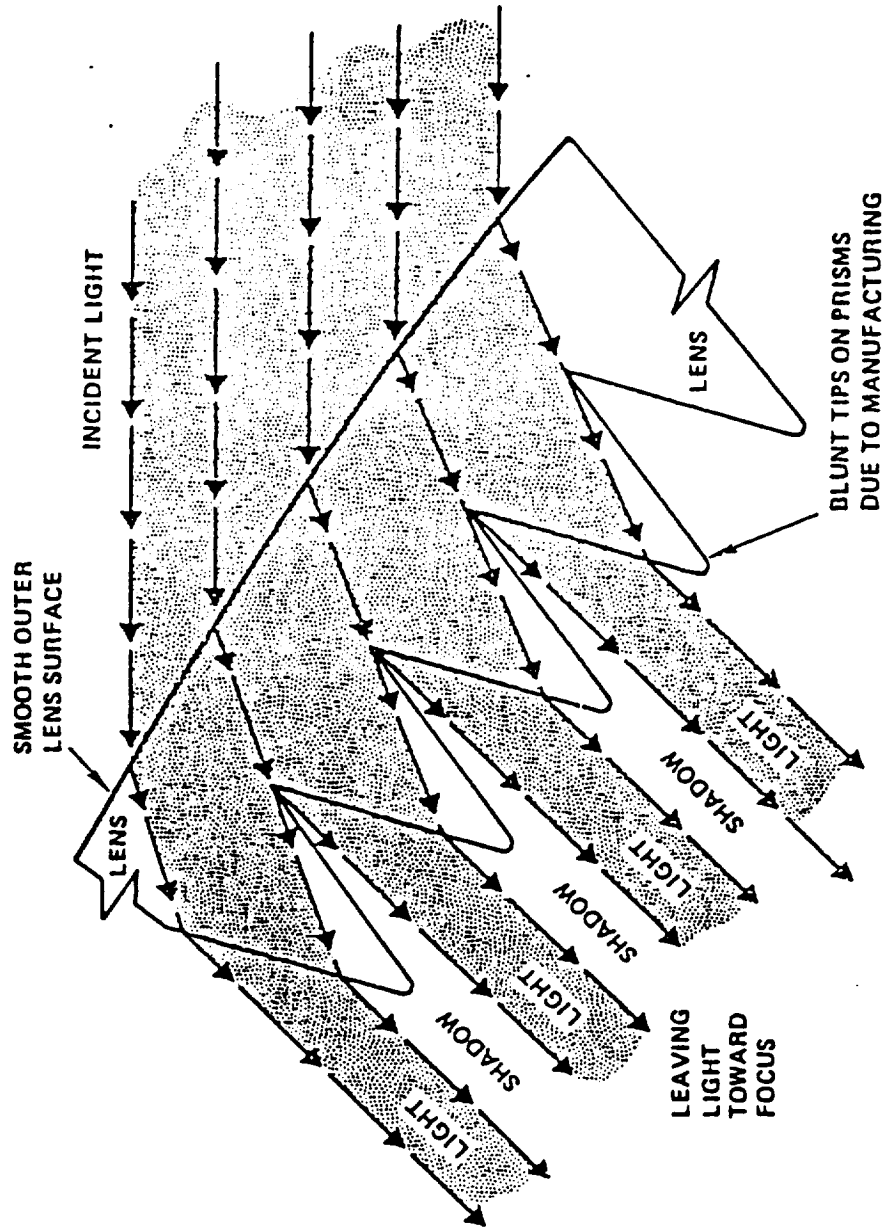
Figure 8

active area of the cell. We next calculated the irradiance distribution over the cell for both perfect sun-pointing and imperfect sun-pointing conditions, using a Monte Carlo ray trace approach, as summarized in Figure 9.

Results of this lens design and analysis effort are shown in Figure 10. With no tracking error, the solar irradiance pattern corresponds to a 2.6 mm diameter circular spot with a peak irradiance of about 300-400 suns. With a 1 degree tracking error, the focal spot moves laterally to the edge of the cell, with negligible loss of photons beyond the cell edge. Neglecting absorption/scattering losses, and assuming a silicone rubber lens without the glass superstrate, the predicted optical efficiency is 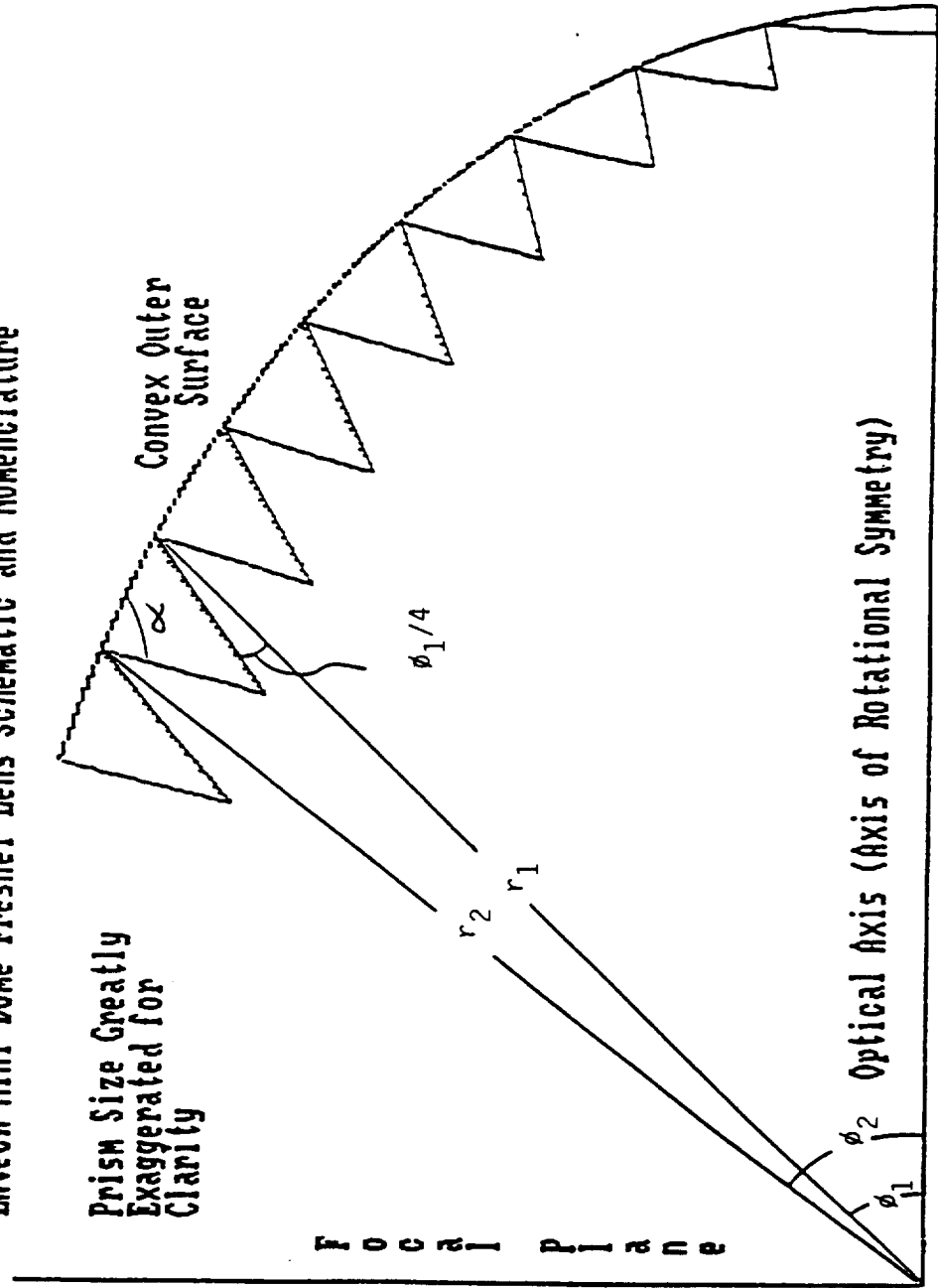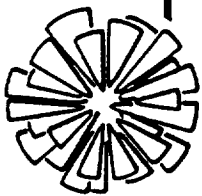about 93%, as shown in Figure 10. However, the glass reflects about 1% more than the silicone rubber, and absorption/scattering losses are expected to be of the order of 1%. Thus, the predicted optical efficiency is about 91%.

Having designed the lens, we next procured a diamond-turned master molding tool from 3M Company. More than a year was required between the placement of the order and the delivery of this unique tool. We provided the lens geometric definition via a computer code, which 3M used to program their world-class diamond turning machine. The resultant lens tool is of exceptional quality.

After receiving the lens tool from 3M, we made prototype silicone rubber lenses (without the glass superstrates) and tested them outdoors with 4 mm diameter gallium arsenide cells. We used opaque shields with square openings to simulate the 3.7 cm by 3.7 cm square aperture of the final lens. Our net optical efficiency measurements were typically in the range of 88% to 91%.

In March 1990, NASA Lewis flew two of our lens/cell prototypes on their Lear Jet High Altitude Test Facility to determine the near-AMO efficiency of the silicone lenses (Reference 12). Figure 11 shows one of the prototype test articles. Figure 12 shows the same test article mounted to the temperature-controlled base plate of a collimating tube which is aimed at the sun during the flight test. Three gallium arsenide cells (4 mm diameter) with similar short-circuit current levels (based on previous simulator testing at NASA Lewis) were used in each test article. The first cell was mounted at the focus of the mini-dome lens. The second cell was mounted to receive full one-sun irradiance even in the presence of a sun-pointing error of several degrees. The third cell was mounted beneath a circular aperture, such that partial shading of this cell would occur if the sun-pointing error exceeded 1 degree. Thus, if the second and third cells had significantly different short-circuit current outputs during the flight test, the tracking error would have exceeded the design value for the lens (as discussed in previous paragraphs). The flight test was conducted by continuously monitoring the short-circuit current of each cell while the altitude was reduced from nearly 50,000 feet to about 35,000 feet. The air mass during the test was determined from the sun angle and barometric pressure during the decrease in altitude. The ratio of the short-circuit currents of the cell at the focus of the lens and the one-sun cell provides a direct measurement of the net concentration ratio provided by the lens. This net concentration ratio was typically between 97 and 98 for both prototypes. The measured aperture area of the square opening in the opaque lens mask was between 108 and 109 times as large as the cell active area for both prototypes; thus, this value is the geometric concentration ratio. The optical efficiency of the lens is determined simply by dividing the net concentration ratio by the geometric concentration ratio. Figures 13 and 14 show the measured optical efficiency as a function of air mass for the two prototypes, respectively. Note that the data are all in the 89-90% range, and that the data

ENTECH, INC.
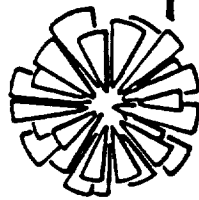
MONTE CARLO RAY TRACE ANALYSIS
FOR SILICONE MINI-DOME FRESNEL LENS

o A NEW DISPERSIVE CONE OPTICS LENS ANALYSIS COMPUTER PROGRAM HAS BEEN WRITTEN TO DESIGN THE MINI-DOME FRESNEL LENS OPTICAL CONCENTRATOR AND TO CALCULATE THE FOCAL PLANE IRRADIANCE PROFILE.

o THE BASIC LENS GEOMETRY IS DEFINED BELOW.

  * FOCAL LENGTH ALONG OPTICAL AXIS: 4.0 CM.
  * LENS SHAPE: ASPHERIC DOME CORRESPONDING TO SYMMETRIC REFRACTION FOR EACH PRISM.
  * SURFACES: SMOOTH CONVEX EXTERIOR WITH PRISMATIC INTERIOR.
  * APERTURE GEOMETRY: 3.7 CM X 3.7 CM SQUARE PROJECTED AREA.

o THE BASIC GALLIUM ARSENIDE CELL GEOMETRY IS DEFINED BELOW.

  * TOTAL ACTIVE AREA: 0.40 CM DIAMETER CIRCLE.
  * GUARD BAND FOR 1 DEGREE TRACKING ERROR: 0.07 CM WIDE ANNULAR RING.
  * TARGET AREA FOR ILLUMINATION WITH NO TRACKING ERROR: 0.26 CM DIAMETER CIRCLE.

o THE PROGRAM FIRST OPTIMIZES THE PRISM ANGLES TO PLACE THE FOCUSSED SUNLIGHT WITHIN THE TARGET AREA, FOLLOWING A "RED-EDGE" DESIGN PHILOSOPHY.

o THE PROGRAM THEN CALCULATES THE FOCAL PLANE IRRADIANCE PROFILE VIA A MONTE CARLO RAY TRACE TECHNIQUE, FURTHER DISCUSSED BELOW.

  * A RAY OF SUNLIGHT IS SELECTED TO EMANATE FROM A RANDOM LOCATION ON THE SOLAR DISK.
  * THE WAVELENGTH OF THE RAY IS RANDOMLY SELECTED FROM THE SPECTRAL PHOTON FLUX PROBABILITY DISTRIBUTION WITHIN THE RESPONSE REGION OF THE GALLIUM ARSENIDE CELL.
  * THE APPROPRIATE REFRACTIVE INDEX IS OBTAINED FROM THE DISPERSION CURVE OF SILICONE.
  * THE RAY INTERCEPTS THE LENS AT A RANDOMLY SELECTED LOCATION ON THE LENS APERTURE.
  * THE RAY TRANSMITTANCE IS CALCULATED FROM THE WELL KNOWN FRESNEL REFLECTION EQUATIONS.
  * A VECTOR RAY TRACE IS CALCULATED TO DETERMINE THE FOCAL PLANE INTERCEPTION POINT.
  * THE RAY IS COLLECTED IN ONE OF THE SMALL FINITE ELEMENT REGIONS IN THE FOCAL PLANE.
  * THE PROCESS IS REPEATED FOR A THOUSAND (OR MORE) RAYS.
  * OUTPUTS INCLUDE THE IRRADIANCE DISTRIBUTION (IN SUNS AS MEASURED BY THE SHORT-CIRCUIT-CURRENT OF A MICROCELL); THE MAPPING OF RAY INTERCEPTS OVER THE CELL; AND THE NET OPTICAL EFFICIENCY OF THE LENS IN DEPOSITING INCIDENT RAYS ONTO THE CELL ACTIVE AREA.

Figure 9

- 14 -

Figure 10

NUMERICAL RESULTS

IRRADIANCE OVER 0.40 CM SQUARE

· 1	1	0	0	0	1	0	2
1	0	6	53	67	10	4	1
1	8	170	150	277	287	13	1
0	63	286	253	274	309	93	0
0	86	312	299	273	326	78	0
1	12	332	391	258	178	9	0
0	4	15	97	82	9	1	1
0	1	0	0	0	1	2	0

4000 RAYS OUT OF 4000
OPTICAL EFFICIENCY TO ACTIVE AREA = .933

4000 RANDOM RAY INTERCEPTS
(ACTIVE AREA CIRCLE DIAMETER = 0.4 CM)
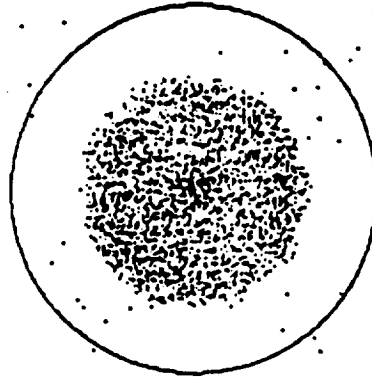
No Tracking Error

NUMERICAL RESULTS

IRRADIANCE OVER 0.40 CM SQUARE

0	0	10	5	57	72	15	5
0	0	31	117	164	303	205	10
0	0	67	281	186	269	365	98
0	0	67	349	295	263	400	87
0	5	15	307	431	210	142	5
0	5	0	10	119	113	15	0
0	0	0	0	0	0	0	0
0	0	0	0	0	0	0	0

1000 RAYS OUT OF 1000
OPTICAL EFFICIENCY TO ACTIVE AREA = .934

1000 RANDOM RAY INTERCEPTS
(ACTIVE AREA CIRCLE DIAMETER = 0.4 CM)
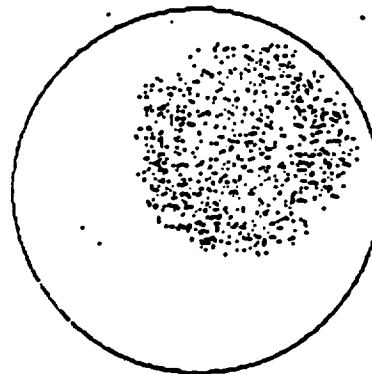
1 Degree Tracking Error

Figure 11 - Prototype Lens/Cell Test Article
for NASA Lewis Lear Jet Flight
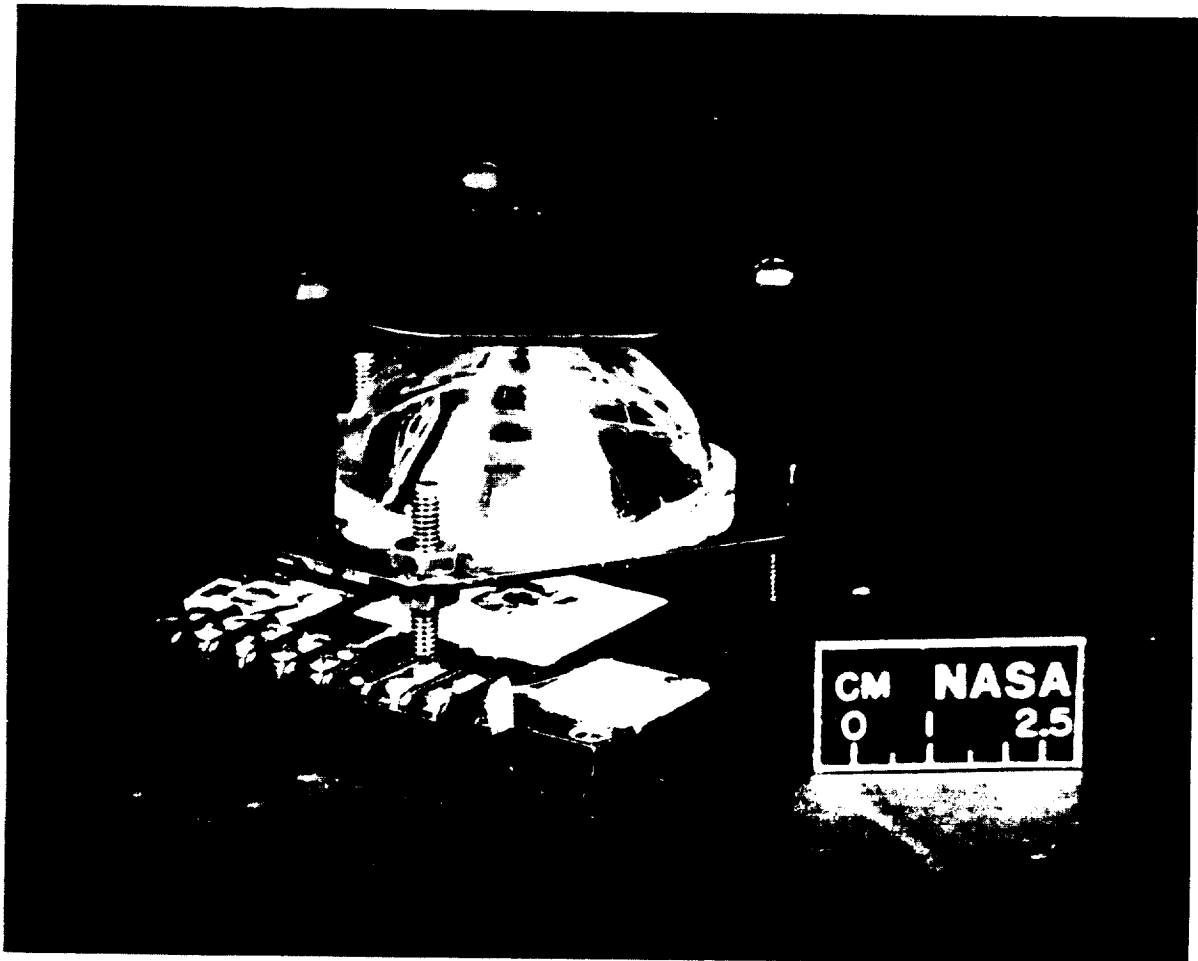
Figure 12 - Prototype Lens/Cell Test Article
Mounted to Collimating Tube Base Plate

ENTECH, INC.
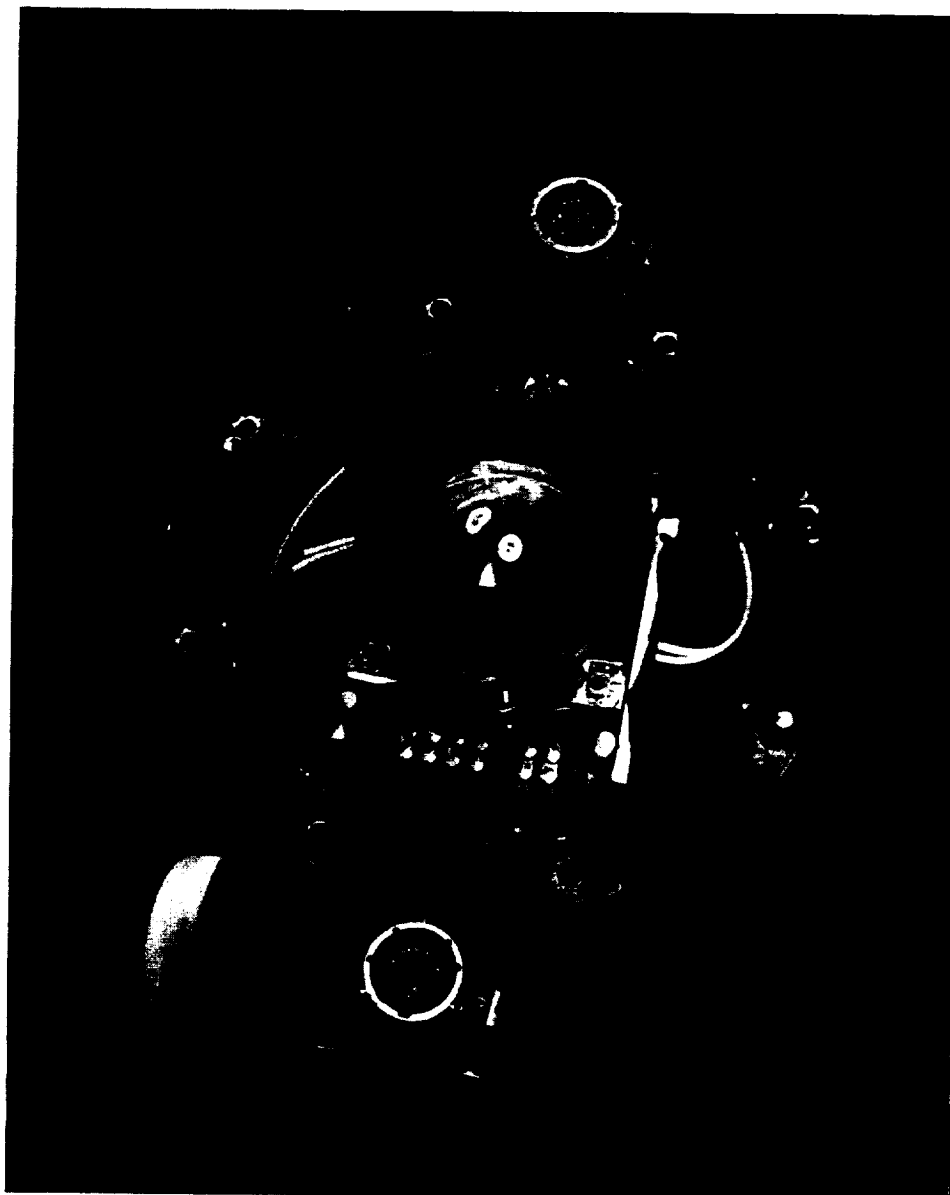
Figure 13

NASA LEWIS LEAR JET HIGH ALTITUDE TEST FACILITY MEASURED LENS PERFORMANCE FOR MODULE #1
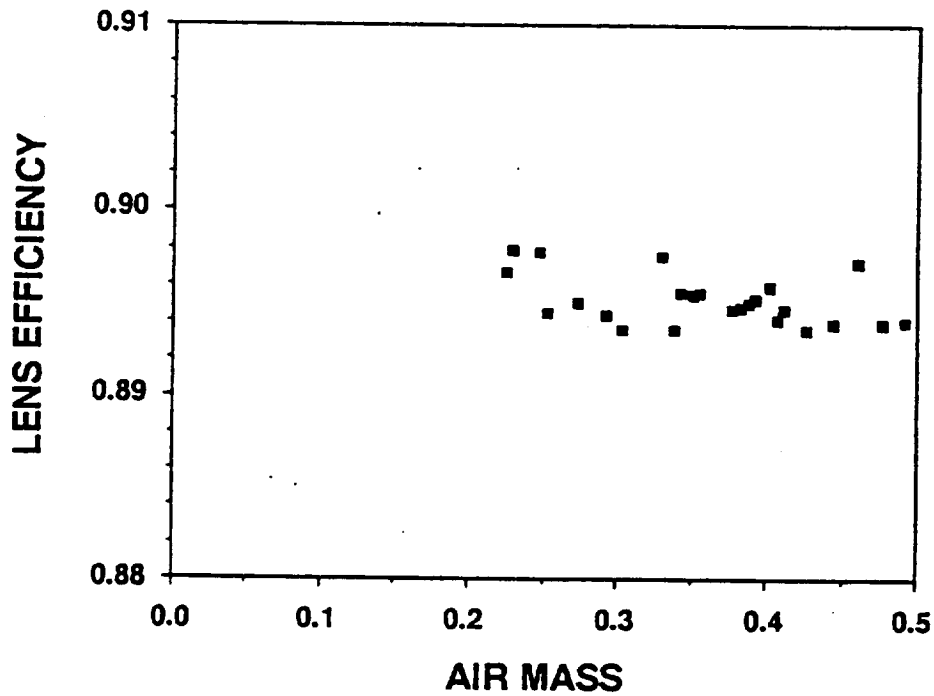
Figure 14

NASA LEWIS LEAR JET HIGH ALTITUDE TEST FACILITY
MEASURED LENS PERFORMANCE FOR MODULE #2
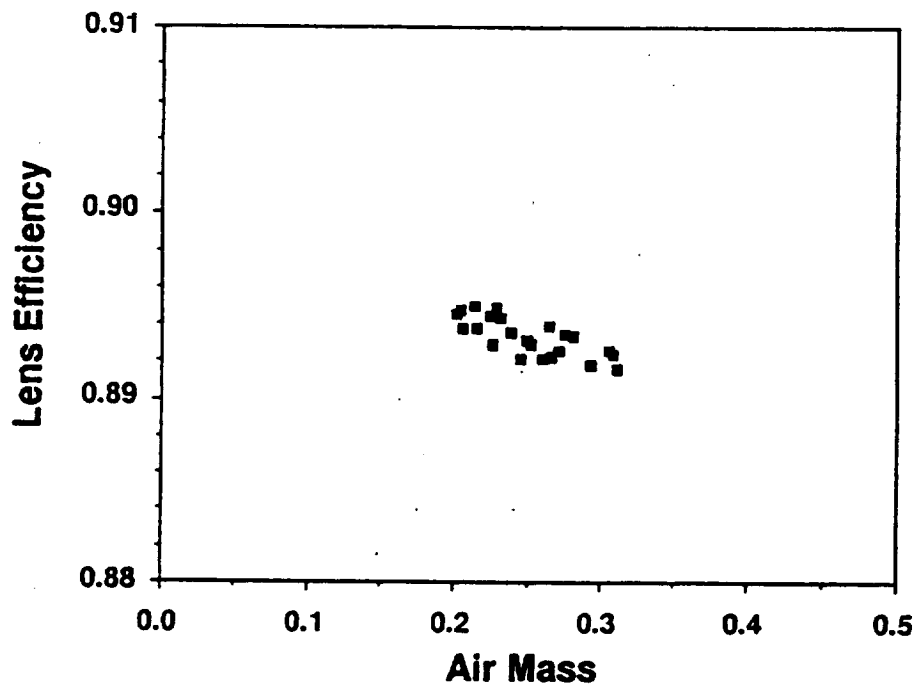
appear to show that lens performance increases slightly with decreasing air mass. NASA's data extrapolations to air mass zero provide net optical efficiency values of 89.8% and 90.0%, for Prototypes 1 and 2, respectively.

Figure 15 summarizes the predicted versus measured lens performance, including both our outdoor tests and NASA's flight tests. (While the initially predicted lens performance in 1986 was for a different polymeric lens material, the lens performance is relatively independent of lens material, provided that the material has optical properties typical of most clear plastics and glasses.)

In addition to on-track optical efficiency, we also measured the off-track tolerance of a mini-dome lens prototype, as summarized in Figure 16. This test was conducted by allowing the sun's image to move completely across the cell, while the prototype was held stationary. The short-circuit current was continuously recorded during the test, while a pyrheliometer was used to verify constant solar irradiance throughout the test. Figure 17 shows the measured response curve. At a full 1 degree tracking error, the cell current output was still within 1% of its on-track value.

In summary, prototype silicone rubber lenses have been tested at 90% net optical efficiency, in close agreement with predicted performance levels. In addition, the off-track performance of prototype lenses has been measured to be in close agreement with predictions.

The above experimental results have been measured for silicone rubber lenses without superstrates. However, we have also made lenses with thin polycarbonate superstrates, which have performed well in lens/cell testing at ENTECH. These polycarbonate/silicone lenses have been used in the prototype panel shown previously in Figure 5, and discussed in more detail in Section 8.0. More recently, we have successfully formed, trimmed, and laminated the desired microglass/silicone lenses. Figure 18 shows one such lens. The current fabrication approach for this lens involves thermal/vacuum forming of flat microglass into the dome shape, using a ceramic mold in a high-temperature kiln; hydrofluoric acid etch-trimming of the full-round glass dome to the final square aperture shape; lamination of a molded full-round silicone lens to the square microglass dome using a thin layer of the outgassed silicone material as the adhesive; and final trimming away of all excess silicone rubber lens material beyond the edges of the square glass superstrate. Optical testing of the glass/silicone lenses will be performed by both ENTECH and NASA under a related on-going project.

Other methods of making the square glass domes have also been explored. Molding of the full-round glass dome is relatively straightforward, and could be accomplished in mass-production using similar equipment to that used to make light bulbs. Trimming of the glass dome to the square shape has proven to be a more difficult problem than making the glass dome. Various trimming systems have been evaluated, including diamond wire saws, abrasive air jets, high-power lasers, and acid etching. The acid etching has a possible advantage in stress relieving the edges, but hydrofluoric acid is a hazardous material. The wire saw approach is relatively slow, and requires significant fixturing. The laser approach causes thermal stress failures. The abrasive air jet approach is still under active development, due to its high speed and low mass production cost potential.

Although the present lens/cell geometry has been selected to provide a 1 degree
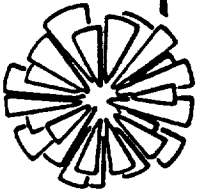
ENTECH, INC.

PREDICTED VERSUS MEASURED OPTICAL EFFICIENCY OF THE MINI-DOME FRESNEL LENS CONCENTRATOR

IN 1986, WE PREDICTED THAT THE SQUARE-APERTURE (3.7 CM BY 3.7 CM) MINI-DOME LENS WOULD PROVIDE 91.5% NET OPTICAL EFFICIENCY WHEN FOCUSSING ONTO A 4 MM DIAMETER GALLIUM ARSENIDE PHOTOVOLTAIC CELL.

IN 1990, WE BUILT TWO PROTOTYPE LENS/CELL UNITS FOR NASA-LEWIS TESTING ABOARD THEIR LEAR JET TO APPROACH AM0 IRRADIANCE CONDITIONS.

BEFORE DELIVERING THE PROTOTYPES TO NASA-LEWIS, WE TESTED THEM OUTDOORS UNDER AM1.5 DIRECT IRRADIANCE AT DALLAS.

WE MEASURED NET OPTICAL EFFICIENCIES OF 88.4% AND 90.5% FOR THE TWO PROTOTYPES.

NASA FLEW BOTH UNITS IN MARCH 1990, AND MEASURED 89.8% AND 90.0% FOR THE TWO PROTOTYPES AT NEAR-AM0 CONDITIONS.

THESE RESULTS ARE SUMMARIZED BELOW.

PREDICTED OPTICAL EFFICIENCY (ENTECH - 1986)	ENTECH-MEASURED AM1.5 OPTICAL EFFICIENCY	NASA-MEASURED AM0 OPTICAL EFFICIENCY
91.5%	88.4 - 90.5%	89.8 - 90.0%

Figure 15

- 21 -
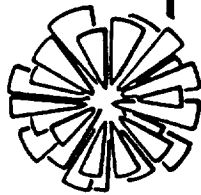
ENTECH, INC.

MEASURED TRACKING ERROR TOLERANCE
FOR MINI-DOME LENS OVER GaAs CELL

TEST METHOD: SQUARE-APERTURE (3.7 CM BY 3.7 CM) DOME LENS, FOCUSSING
ONTO 4 MM DIAMETER GaAs CELL (NO PRISM COVER).
LENS/CELL MOUNTED ON PYRHELIOMETER TRACKER OUTDOORS AT ENTECH.
LENS/CELL UNIT ROTATED ABOUT POLAR AXIS SLIGHTLY WEST OF SUN.
TRACKER MOTOR TURNED OFF. SUN'S IMAGE ALLOWED TO PASS OVER CELL.
CELL CURRENT VERSUS TIME RECORDED. TEST DATE 3/15/90.
SUN'S ANGULAR MOTION = 0.25 DEGREES PER MINUTE FOR TEST DATE.
RESULTS PRESENTED BELOW.

SUN POINTING ERROR	RELATIVE CELL CURRENT OUTPUT
(DEGREES)	(PERCENT)
0.00	100.0
± 0.25	100.0
± 0.50	100.0
± 0.75	99.7
± 1.00 (*** DESIGN VALUE ***)	99.0 (*** 100.0% PREDICTED ***)
± 1.25	97.4
± 1.50	92.8
± 1.75	83.9
± 2.00	74.6

Figure 16

- 22 -

Figure 17

TRACKING ERROR PERFORMANCE TEST
FOR PROTOTYPE MODULE #1
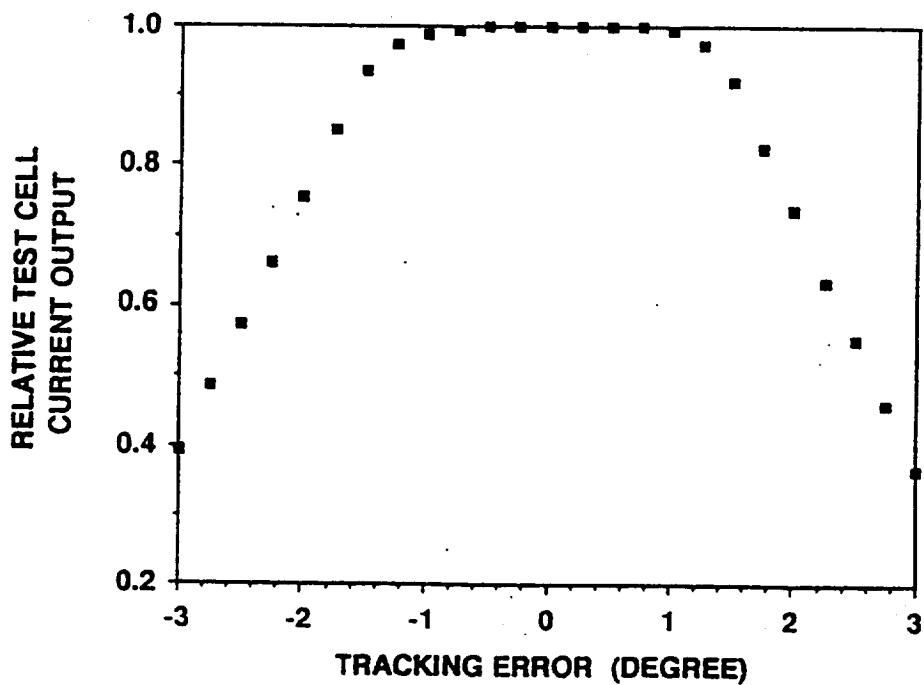
LENS/CELL ELEMENT DESIGNED
FOR 1 DEGREE TRACKING ERROR TOLERANCE

ENTECH, INC.

Figure 18 - Laminated Ceria Microglass/Silicone Fresnel Lens Approach:

      1.   Upper Left Is Full-Round Glass Dome.

      2.   Lower Left Is Square-Cut Glass Dome.

      3.   Upper Right Is Full-Round Silicone Lens.

      4.   Lower Right Is Laminated Glass/Silicone Lens.
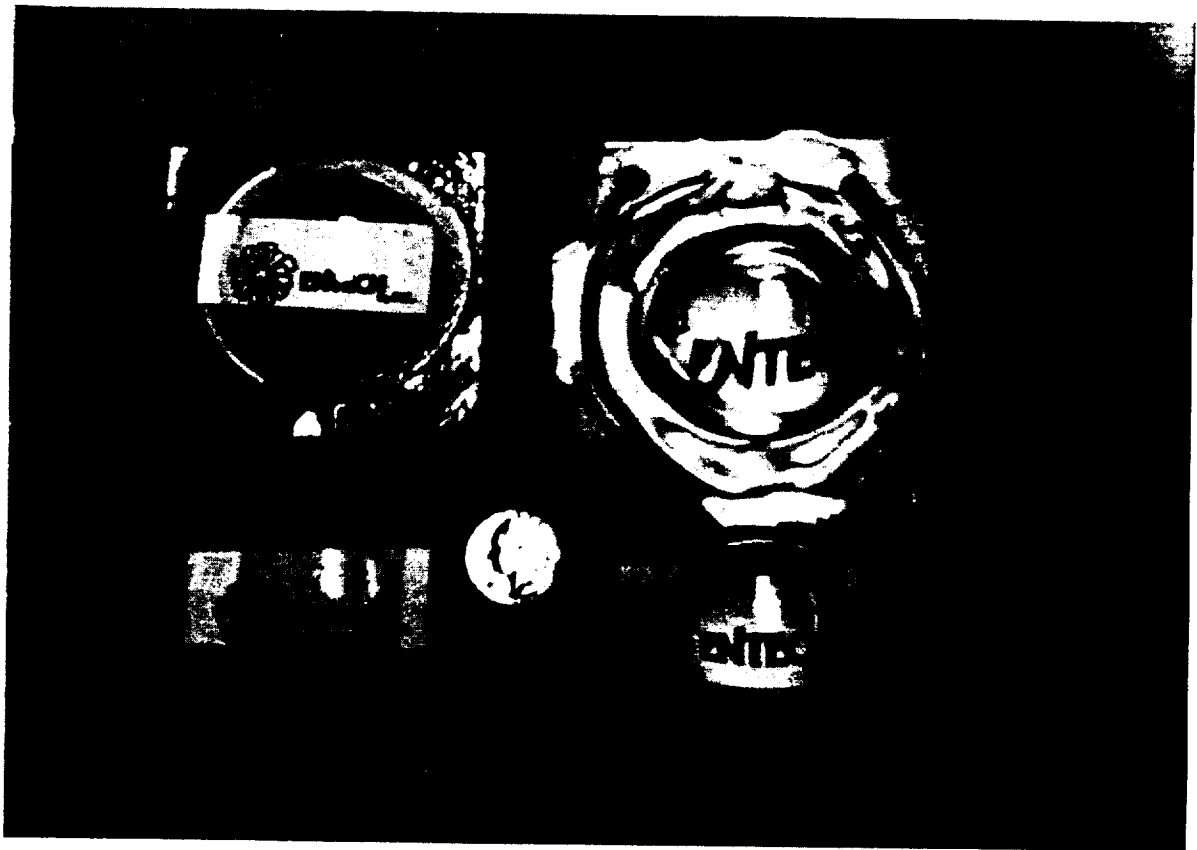
sun-tracking error tolerance, larger tolerances can be achieved by merely making the cell diameter larger. Figure 19 shows the small penalty in performance that results from oversizing the cell to achieve higher tracking error tolerance levels. Figure 19 is taken from our Phase I final report (Reference 1), and includes the gridline lengthwise resistance increase with larger cell diameter, as well as the open circuit voltage reduction resulting from a larger cell size (more dark current). Thus, the existing lens can be used with various cell sizes to provide a wide range of sun-tracking tolerance levels.
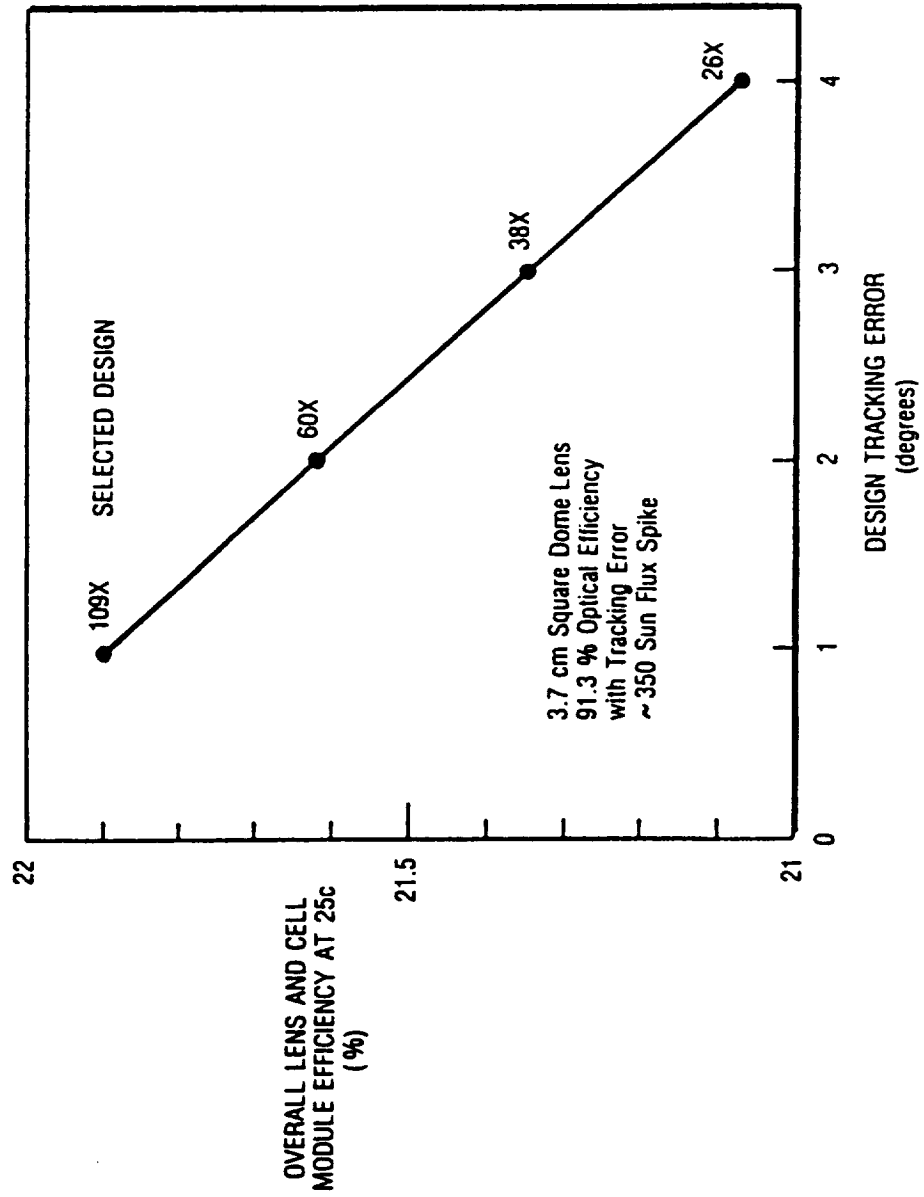
Figure 19

4.0 Prismatic Cell Cover Development

Figure 20 is a cross-sectional schematic of our patented prismatic photovoltaic cell cover. Our present covers are made from the same silicone material used in the mini-dome Fresnel lens. This material was selected for its moldability, flexibility (minimizing cell stresses), and history of use in space. The transparent cover comprises a multitude of parallel miniature lenses which focus incident light between gridlines, thereby avoiding the normal gridline obscuration loss. Figure 21 shows ray traces through the cover for rays coming from various portions of the mini-dome lens primary optical concentrator. Note that the cover is able to refract rays coming from all portions of the mini-dome lens such that they avoid interception with the gridlines. The cover design shown in Figure 21 is the result of a parametric optimization analysis which considered a variety of individual optical element configurations. The selected design provides the highest gridline coverage fraction while fully eliminating the gridline shadowing loss. The select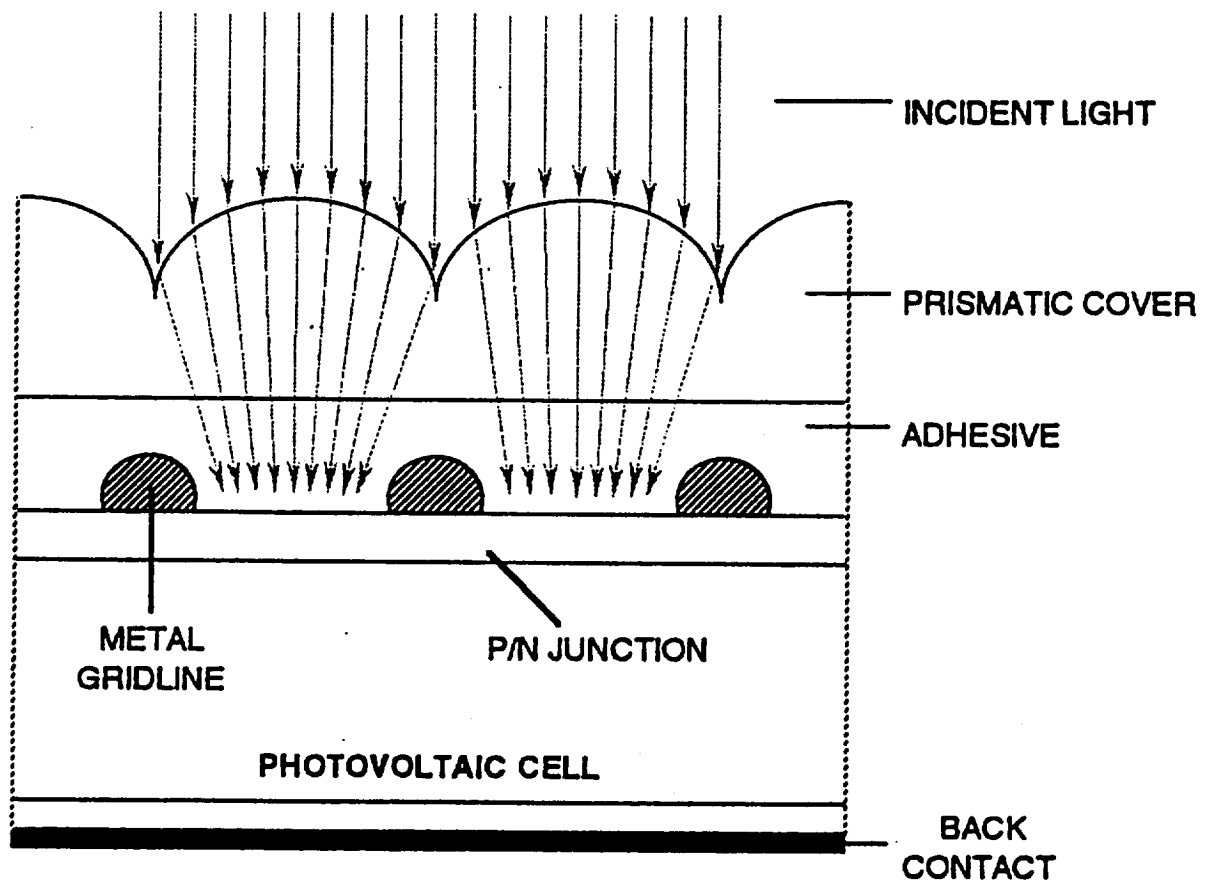ed design would allow 15% gridline coverage of the illuminated top surface of the cell. However, to provide prism cover/cell alignment tolerance, we selected about 10% gridline coverage for the cell design (12 micron wide gridlines on 127 micron centers), as further described in Section 5.0 (Figure 23). For the selected design, each cylindrical optical element (Figure 20) in the prism cover is 127 microns wide by about 80 microns thick, including silicone adhesive.

Having designed the prismatic cover, we procured diamond-machined tooling from Fresnel Optics. When the tooling was delivered, we fabricated covers for evaluation. The effectiveness of these prismatic cell covers was verified by NASA Lewis by testing the same cells in a solar simulator before and after prismatic cover application by ENTECH. Figure 22 shows a typical result of such bare versus covered cell tests. The prismatic cover increased the current output and the efficiency of the cell by 12% and 11%, respectively. For a 10% metal coverage, the theoretical gain for the cover is 11%, since the cover should increase the unshaded active cell area from 90% to 100% of the total cell active area (i.e., 100/90 = 1.11). Thus, the cover performance is very close to ideal.

One might ask why reflection from the outer surface of the cover should not reduce the prism cover gain by 3-4%. The answer is that such a loss does occur. However, this loss is essentially offset by a beneficial reduction in the reflection loss from the top surface of the antireflection coating on the cell. When the prism cover is bonded to the outer surface of the antireflection coating on the cell, the reflection coefficient for this surface is typically reduced, compared to its previous value with air (or vacuum) in contact with the antireflection coating. The reflection coefficient for a surface depends on the difference between the refractive indices on either side of the surface. Air (or vacuum) has a refractive index of about 1, while the silicone prism cover material has a refractive index of about 1.4. The outer layer of most antireflection coatings has a refractive index closer in value to the refractive index of silicone rubber than to the refractive index of air (or vacuum). Thus, the prism cover generally reduces the reflection loss from the antireflection coating by several percent, compared to the bare cell reflection loss. This improvement usually offsets the reflection loss from the outer surface of the prism cover, allowing the cover to achieve gain factors in close agreement with complete elimination of gridline shadowing losses.

By using the prismatic covers, unprecedented space solar cell efficiency levels have been achieved, as further discussed in the following section.

Figure 20 - Cross-Sectional Schematic of ENTECH's Patented
             Prismatic Cell Cover (U.S. Patent No. 4,711,972

INCIDENT LIGHT

PRISMATIC COVER

ADHESIVE

METAL
GRIDLINE

P/N JUNCTION

PHOTOVOLTAIC CELL

BACK
CONTACT

Note: Total Cover Thickness, Including Adhesive, Is 80 Microns.
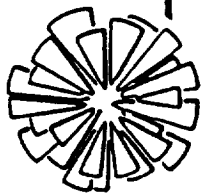
ENTECH, INC.

ENTECH, INC.

RAY TRACES SHOWING HOW THE PRISM COVER ELIMINATES
GRIDLINE SHADOWING LOSS AT THE CELL FOR RAYS
COMING FROM VARIOUS PORTIONS OF THE MINI-DOME LENS

Rays from
Center of Lens
(0° Incidence)

Rays from Upper
Edge of Lens
(30° Long. Inc.)

Rays from Right
Edge of Lens
(30° Lat. Inc.)

Rays from Upper
Right Corner of Lens
(51° Diag. Inc.)

Grid   Grid   Grid   Grid   Grid   Grid
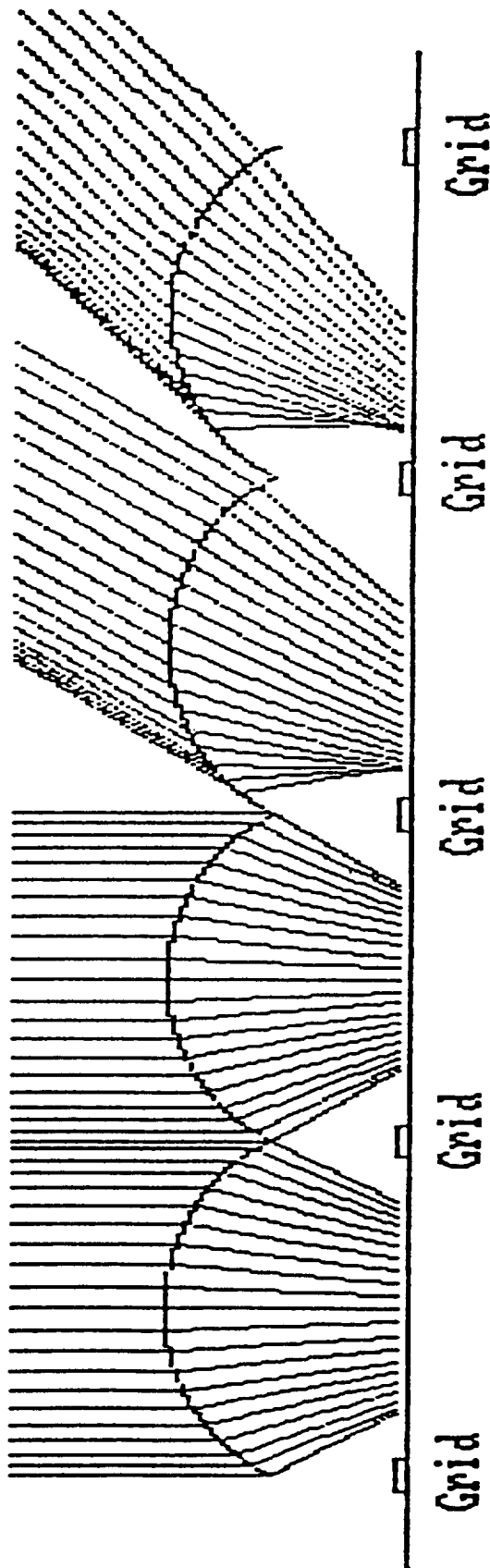
Gallium Arsenide Cell with 12 micron wide Grids on 127 micron Centers

Figure 21

- 29 -

NASA-MEASURED AMO CELL PERFORMANCE BEFORE AND AFTER PRISMATIC COVER APPLICATION

NASA-LEWIS AMO SIMULATOR
100 SUNS IRRADIANCE = 137,100 W/SQ.M.
25 C CELL TEMPERATURE
CELL NO. 25 (BARE VS. PRISM-COVERED)
CELL AREA = .1257 SQ.CM.

	ISC	VOC	FF	EFFICIENCY
BARE CELL	0.377 A	1.145 V	86.7%	21.8%
COVERED CELL	0.423 A	1.143 V	86.1%	24.2%
GAIN FACTOR	1.122	0.998	0.993	1.110

Figure 22

- 30 -

5.0 Photovoltaic Cell Development

During Phase I of this NASA SBIR project, we selected a gallium arsenide cell for use in the mini-dome lens concentrator system, based on efficiency, radiation hardness, high temperature capability, and technological maturity. As described in Section 5.1 below, we procured gallium arsenide cells from Varian Associates, applied prismatic covers to these cells, and demonstrated world record performance levels in simulator tests at NASA Lewis. In addition, last year we began a collaboration with Boeing on their exciting new mechanically stacked multi-junction (tandem) cell. The Boeing tandem cell concept maintains the excellent performance of the gallium arsenide cell, despite making it transparent to infrared radiation, and adds to that performance with a second infrared-responsive gallium antimonide cell located behind the gallium arsenide cell. When both cells are equipped with our prismatic cell covers, truly remarkable performance levels have been achieved, as further discussed in Section 5.2 below. Fortunately, both types of cells, as well as numerous other types (including indium phosphide and monolithic tandem cells) can be readily incorporated into the mini-dome lens concentrator system.

5.1 Varian Gallium Arsenide Cell

During Phase I of this NASA SBIR project, we conducted parametric analyses of the gallium arsenide solar cell to quantify the effect of cell size, irradiance distribution, and gridline pattern geometry on cell performance (Reference 1). Based on the results of these studies, and on the practical consideration that several organizations had been developing 4 mm diameter concentrator cells under other NASA and DOD projects, we selected the cell design shown in Figure 23. We procured cells from Varian Associates based on this design. After prismatic cell covers were applied to these cells, NASA Lewis measured the performance of these cells in their AMO solar simulator. Measured performance parameters for one of these cells are shown in Figure 23, as well as predicted performance parameters. Note that the measured cell efficiency was over 24% at 25C and 100 AMO suns irradiance, as predicted. Note also that the measured cell efficiency was approximately 22% at 100C and 100 AMO suns, also as predicted. Both of these results, when measured, set new world records for space cells of any kind. As of this writing, these results still represent world records for single-junction space cells. However, the Boeing tandem cell discussed in the following section has established an impressive new world record for a space cell of any kind.

5.2 Boeing Tandem Gallium Cell

In the spring of 1989, Lew Fraas and his colleagues at Boeing perfected the new mechanically stacked multi-junction (tandem) cell comprising an infrared-transparent gallium arsenide top cell and an infrared-responsive gallium antimonide bottom cell. We supported the Boeing team by making and applying prismatic covers to both the top and bottom cells in several prototype cell assemblies. Under simulated AMO sunlight concentration, the new Boeing cell has demonstrated about 24% top cell efficiency plus about 7% bottom cell efficiency, for a total cell efficiency of 31%, in tests conducted by NASA Lewis. The bottom cell current response was also calibrated by flying sample cells under gallium arsenide filters aboard the NASA Lewis Lear jet to approach AMO spectral conditions.

Therefore, by simply substituting the new Boeing tandem gallium cell in place of the gallium arsenide cell, the mini-dome lens concentrator system can provide

ENTECH/VARIAN GALLIUM ARSENIDE CELL AND PREDICTED VERSUS NASA-MEASURED PERFORMANCE AFTER PRISMATIC COVER APPLICATION
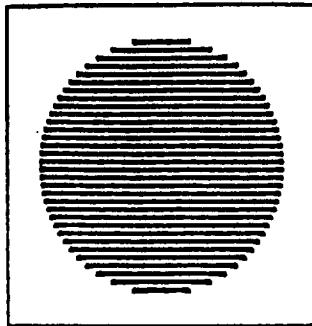
GEOMETRY TOTAL AREA: SQUARE, 0.5 CM PER SIDE.
ACTIVE AREA: CIRCLE, 0.4 CM DIAMETER.

METALLIZATION GRIDLINES: 31 PARALLEL LINES ON 127 MICRON CENTERS, EACH 12 MICRONS WIDE BY 5 MICRONS TALL.

BUSBAR: CONTINUOUS AROUND CELL PERIPHERY.

PREDICTED VS. MEASURED CELL PERFORMANCE AT STANDARD TEST CONDITIONS

(100 UNIFORM AMO SUNS, 25C CELL TEMPERATURE)

PARAMETER	PREDICTED VALUE	NASA-MEASURED VALUE
SHORT-CIRCUIT CURRENT:	0.415 AMP	0.423 AMP
OPEN-CIRCUIT VOLTAGE:	1.154 VOLTS	1.143 VOLTS
FILL FACTOR:	87.5 %	86.1 %
CELL EFFICIENCY:	24.3 %	24.2 %

PREDICTED VS. MEASURED CELL EFFICIENCY AT ORBITAL OPERATING TEMPERATURE

(100 UNIFORM AMO SUNS, 100C. CELL TEMPERATURE)

PREDICTED CELL EFFICIENCY: 21.7%
NASA-MEASURED CELL EFFICIENCY: 21.9%

Figure 23

nearly one-third higher power output with the same area and mass. In addition, Boeing has assured us that the new cell is readily producible. Furthermore, even higher performance levels are expected in the near future, as the gallium antimonide cell continues to improve in technological maturity. The exciting new Boeing cell has been described in several recent publications (e.g., References 13 and 14).

6.0 Cell Mount/Interconnect Development

During Phase I of this SBIR program, we defined the functional and material requirements of the cell-to-radiator mounting system, as shown in Figure 24. The cell must be electrically isolated from the backplane radiator, while maintaining an excellent thermal conduction path to the same radiator. A thermally conductive dielectric material such as alumina is therefore required between the cell and radiator. Ideally, a thin layer of alumina should be applied to the radiator at the cell mount location by a deposition technique such as plasma spraying, to minimize thermal contact resistance at the alumina/aluminum interface. Next a solderable metal pad should be applied to the upper surface of the alumina, followed by cell soldering to the metal pad. Such a cell mount should provide a reasonable 4 degree C cell-to-radiator temperature difference at the center of the cell, where a 350 sun peak irradiance exists, based on the one-dimensional heat conduction analysis of Figure 24.

For prototype cell assemblies produced during Phase II of the program, we jointly decided with NASA Lewis personnel to use a lower risk cell mount approach which has been successfully used in terrestrial photovoltaic concentrators (Reference 9). In this approach, the cell is directly soldered (using SN-62 solder) to a thin (175 micron) copper sheet which is significantly larger (12.7 mm square) than the cell. Thus, the copper serves as a heat spreader. The copper heat spreader is then bonded to the backplane radiator with a thin (125 micron) alumina-loaded silicone rubber adhesive. While the alumina-loaded adhesive has an order-of-magnitude lower thermal conductivity than pure alumina, the larger conduction area provided by the heat spreader offsets this property disadvantage. This cell/copper/adhesive mounting approach was used throughout Phase II for prototype test articles, including the lens/cell test articles flown on the NASA Lear jet (discussed in Section 3.0) and the prototype panels (discussed in Section 8.0). The top contact to these prototype cells was made by soldering a 75-micron diameter copper wire to each of the four corners of the peripheral busbar on the top surface of the cell (Figure 23). These wires were then soldered to a copper top interconnect tab. Cell-to-cell interconnection was then done by soldering copper wires to the front copper interconnect tab (for a negative connection) and the back copper heat spreader (for a positive connection). (Photos of such connections are shown in Section 8.0).

Late in the Phase II program, NASA Lewis personnel discovered that the cell-to-heat spreader joint mechanically and electrically degraded after several thousand thermal cycles, and will therefore require further development to improve reliability, if this approach is selected for later hardware. However, in our on-going collaboration with Boeing relative to the use of their tandem gallium cell in our mini-dome concentrator panels, they have proposed a wire-bonded flex-circuit approach to cell mounting and interconnection (Reference 14). Thus, new materials and techniques are currently being developed for this tandem cell application.
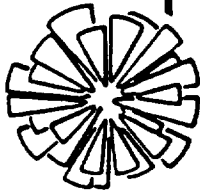
ENTECH, INC. CELL MOUNT THERMAL ANALYSIS

Heat Flux

Q̇

Solder

Ga As Cell

Plasma-Sprayed Alumina
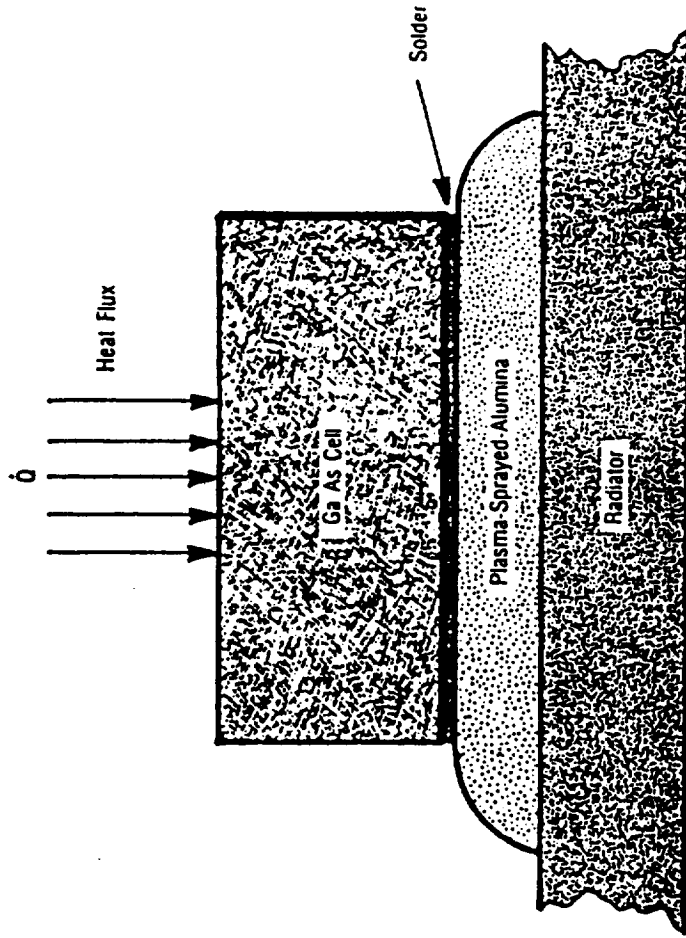
Radiator

ELEMENT	THICKNESS	THERMAL CONDUCTIVITY	l/k
Cell	0.0305 cm	0.39 w/cm °c	0.078 cm²·°c/w
Solder	0.0025 cm	0.32 w/cm °c	0.008 cm²·°c/w
Alumina	0.0127 cm	0.35 w/cm °c	0.036 cm²·°c/w
Radiator	0.0102 cm*	1.73 w/cm °c	0.006 cm²·°c/w
		TOTAL	0.128 cm²·°c/w

Q̇ = 350 suns · 0.1353 w/cm² · (0.95 · 0.24) = 33.6 w/cm²

Tcell · Tradiator = Q̇ · l/k = 4.3°c

* ½ thickness of radiator, since heat radiates from both sides, and average radiator temperature is of interest.

Figure 24

7.0 Radiator/Honeycomb Development

During Phase I of this SBIR project, we selected the all-aluminum square honeycomb/backplane radiator structural/thermal approach for the mini-dome lens panel, based on its simplicity, light weight, low cost, good rigidity, and excellent heat transfer. We assumed that the simplest way to make such an aluminum honeycomb/radiator assembly was to fabricate thin sheets of aluminum and to bond them together into the final configuration. During Phase II, we actually made prototype aluminum parts, and adhesively bonded them together to form such a panel structure. However, this approach was time-consuming and clearly would require sophisticated fixturing to implement on a production basis.

In our collaboration with Boeing, relative to the use of our prism covers on their tandem gallium arsenide/gallium antimonide cells in our mini-dome lens concentrator panel, we showed them the prototype panel structure and discussed its fabrication requirements. Shortly after this discussion, Bill Yerkes of Boeing began to investigate the use of a computer-controlled milling machine to cut a single-piece honeycomb/radiator panel structure out of a thick plate of aluminum. At Boeing, such a machine was programmed and trial cutting runs were made. First, an individual square slot was cut into a plate of aluminum. Next, three side-by-side elements were cut into a plate (See Figure 27 in Section 8.0). Finally, a full six-by-six element square panel was cut into a plate of aluminum. (Photos of such a panel are shown in Figures 28-31 of Section 8.0). This machining approach to panel structure fabrication is surprisingly quick and cost-effective. Each square element is completely cut out in less than five minutes (at a cost of less than $5 in machine time). The resultant aluminum shavings (which can be re-cycled) weigh less than one-third pound per square element, corresponding to a material cost of less than $0.50 per element.
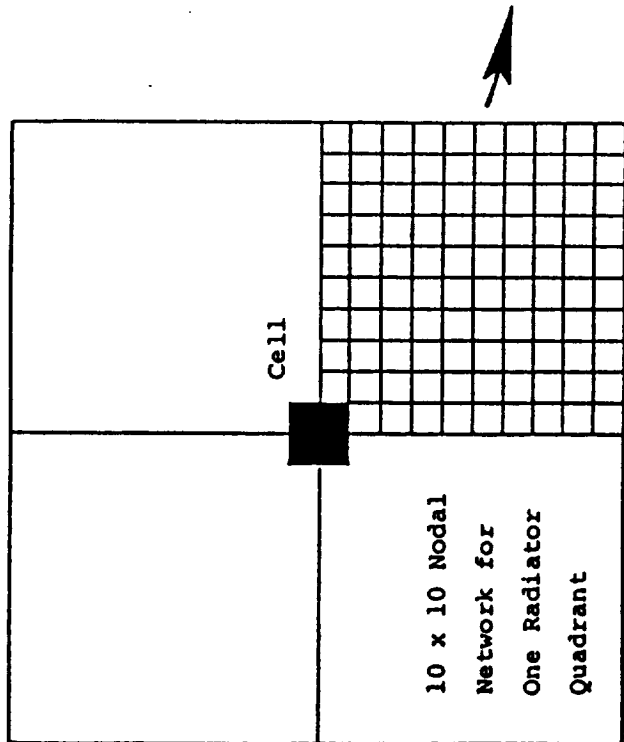
The machined panel approach offers many benefits over other fabrication techniques. Structurally, the unitized aluminum honeycomb/backplane panel is ideal. Thermally, the machining approach offers the potential to taper the backplane radiator, making it thicker near the cell mount where the maximum radial heat conduction occurs, and thinner near the adiabatic boundaries of the square slot. Mechanically, the machining approach allows mounting ledges, lightening holes, gussets, flanges, and other desirable geometrical features to be added by simple programming changes. Economically, the machining approach can be combined with isotropic acid etch thinning to provide the lowest possible panel weight; since each pound of launch weight reduction equates to several thousand dollars of mission cost savings, this is probably the greatest benefit of the panel machining approach.

During Phase I of this SBIR project, we conducted thermal analyses of the radiator to define the effect of radiator thickness on cell operating temperature. These analyses have been refined during Phase II, and Figures 25 and 26 present typical results for two very different radiator thicknesses (200 microns and 50 microns, respectively). These results are for the hottest portion of a low earth orbit (LEO) mission, when the fully sun-illuminated earth is directly behind the mini-dome lens panel. These results are for a gallium arsenide single-junction cell; temperatures would be lower for the Boeing tandem cell, since its higher conversion efficiency reduces the waste heat load on the radiator. Note that the hottest region of the radiator, directly below the cell, is about 96 degrees C for the 200 micron thick radiator, and about 130 degrees C for the 50 micron thick radiator. Adding the 4 degrees C cell-to-radiator temperature difference (discussed in Section 6.0), we can see that the maximum
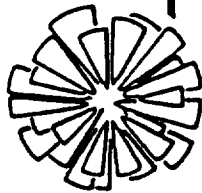
ENTECH, INC.

THERMAL ANALYSIS RESULTS FOR A
0.020 CM (0.008 INCH) THICK RADIATOR

QUADRANT TEMPERATURES (C)

95.815	91.368	88.749	87.015	85.788	84.894	84.244	83.788	83.497	83.355
91.368	89.640	87.960	86.601	85.547	84.741	84.140	83.712	83.436	83.301
88.749	87.960	86.945	85.977	85.147	84.474	83.953	83.572	83.324	83.202
87.015	86.601	85.977	85.307	84.683	84.146	83.714	83.390	83.175	83.068
85.788	85.547	85.147	84.683	84.221	83.803	83.455	83.187	83.007	82.916
84.894	84.741	84.474	84.146	83.803	83.482	83.204	82.986	82.837	82.761
84.244	84.140	83.953	83.714	83.455	83.204	82.982	82.805	82.681	82.618
83.788	83.712	83.572	83.390	83.187	82.986	82.805	82.657	82.553	82.500
83.497	83.436	83.324	83.175	83.007	82.837	82.681	82.553	82.463	82.416
83.355	83.301	83.202	83.068	82.916	82.761	82.618	82.500	82.416	82.372

Cell

10 x 10 Nodal

Network for

One Radiator

Quadrant

ASSUMPTIONS: White Thermal Control Coating on Both Sides of Radiator
(Solar Absorptance = 0.20, Infrared Emittance = 0.90 ,
Aluminum Radiator Thermal Conductivity = 173 w/m-K)

Transparent Dielectric Lens Material
(Solar Transmittance = 0.92, Infrared Emittance = 0.9)

Low Earth Orbit, Radiator Facing Earth, Lens Facing Sun
(Solar Constant = 1371 w/sq.m., Earth Albedo Reflectance = 0.36,
Earth Effective Radiation Temperature = 255K,
Radiator-to-Earth View Factor = 0.96)

Prism-Covered GaAs Cell
(Solar Absorptance = 0.95, Electrical Conversion Efficiency = 0.20,
Cell Area = 0.01 times Lens Area)

Net Heat Rate from Cell to Radiator
(3.7 cm x 3.7 cm x 0.1371 w/sq.cm. x 0.92 x (0.95 - 0.20) = 1.30 w)

Figure 25

- 37 -

THERMAL ANALYSIS RESULTS FOR A
0.005 CM (0.002 INCH) THICK RADIATOR

ENTECH, INC.
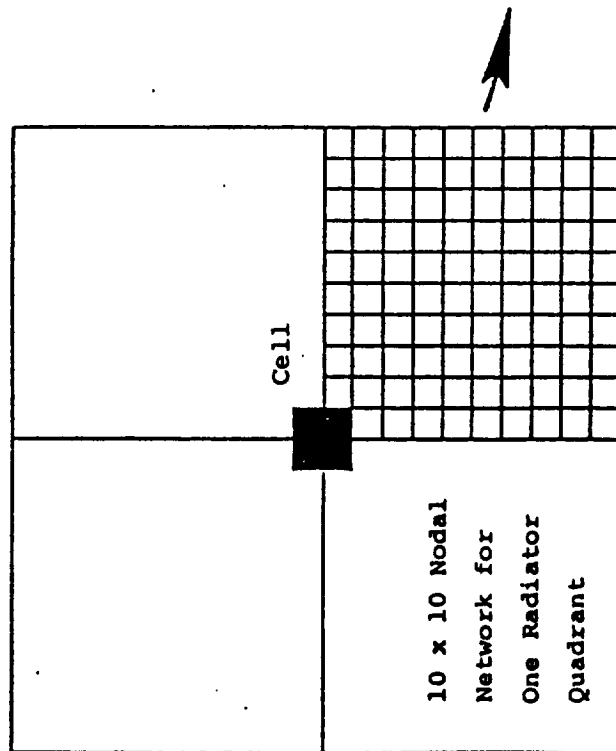
QUADRANT TEMPERATURES (C)

129.610	111.940	101.624	94.859	90.118	86.694	84.223	82.498	81.403	80.870
111.940	105.117	98.535	93.256	89.192	86.114	83.832	82.216	81.181	80.675
101.624	98.535	94.587	90.848	87.667	85.104	83.131	81.700	80.769	80.311
94.859	93.256	90.848	88.279	85.900	83.868	82.239	81.026	80.223	79.824
90.118	89.192	87.667	85.900	84.152	82.583	81.277	80.279	79.607	79.270
86.694	86.113	85.104	83.868	82.583	81.380	80.348	79.540	78.987	78.707
84.222	83.832	83.131	82.239	81.277	80.348	79.529	78.875	78.421	78.189
82.498	82.216	81.700	81.026	80.279	79.540	78.875	78.335	77.956	77.761
81.403	81.181	80.769	80.223	79.607	78.987	78.421	77.956	77.626	77.456
80.870	80.675	80.311	79.824	79.270	78.707	78.189	77.761	77.460	77.302

Cell

10 x 10 Nodal Network for One Radiator Quadrant

ASSUMPTIONS: White Thermal Control Coating on Both Sides of Radiator
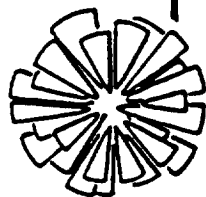(Solar Absorptance = 0.20, Infrared Emittance = 0.90, Aluminum Radiator Thermal Conductivity = 173 w/m-K)

Transparent Dielectric Lens Material
(Solar Transmittance = 0.92, Infrared Emittance = 0.9)

Low Earth Orbit, Radiator Facing Earth, Lens Facing Sun
(Solar Constant = 1371 w/sq.m., Earth Albedo Reflectance = 0.36, Earth Effective Radiation Temperature = 255K, Radiator-to-Earth View Factor = 0.96)

Prism-Covered GaAs Cell
(Solar Absorptance = 0.95, Electrical Conversion Efficiency = 0.20, Cell Area = 0.01 times Lens Area)

Net Heat Rate from Cell to Radiator
(3.7 cm x 3.7 cm x 0.1371 w/sq.cm. x 0.92 x (0.95 - 0.20) = 1.30 w)

Figure 26

cell operating temperature will be about 100 degrees C for the thicker radiator, and about 134 degrees C for the thinner radiator. These gallium arsenide cell temperature levels correspond to efficiency values of about 22% at 100 degrees C and about 21% at 134 degrees C, based on the NASA cell measurements discussed in Section 5.1. Thus, the selection of an optimum radiator thickness is a complex tradeoff between cell performance and radiator mass. Since residual atmospheric drag is a critical factor in long-term LEO missions, such as the Space Station Freedom, this factor must be thoroughly considered in making such a selection. We currently consider the thicker radiator as our NASA baseline design, while the thinner radiator is being investigated for an ultra-light version of our panel for SDIO applications.

The thermal analyses discussed above are conservative. The simple thermal model treats the heat transfer from the lens-side of the radiator as one-dimensional radiation between separated parallel plates, i.e., the radiator radiates heat to the lens, which subsequently radiates heat to deep space. In reality, the vertical honeycomb walls between the radiator and the lens can be designed to significantly enhance the lens-side heat rejection via both conduction and radiation. Similarly, other array design improvements (e.g., tapering of the backside radiator) are expected to further reduce the cell operating temperature level for later flight versions of the mini-dome lens array. Furthermore, the analyses presented above are for the hottest instant in the hottest orbit (LEO). In contrast, preliminary calculations indicate that the cell operating temperature will be about 20 degrees C lower for geosynchronous orbit (GEO) than for LEO.

8.0 Prototype Concentrator Panel Development

In collaboration with Boeing, we fabricated several three-element mini-panels to demonstrate the basic mini-dome lens photovoltaic concentrator panel approach. One such mini-panel is shown in Figure 27. The integral honeycomb/radiator structure was machined from a plate of aluminum (as described in Section 7.0). The lenses were made by first molding a round silicone rubber lens, by next bonding the lens to a squared dome superstrate (using outgassed silicone as the adhesive), and by finally trimming away the excess silicone lens material beyond the square edges of the superstrate. For these prototype panels, polycarbonate superstrates were used in place of the preferred ceria microglass superstrates, due to ease of fabrication, as well as project cost and schedule constraints. (The polycarbonate superstrates also served as a good learning tool for lamination and assembly, while we sought to perfect the microglass superstrates.) The cells in these mini-panels were non-functional chips which simulated the Boeing tandem gallium cells in configuration.

After delivering one of these three-element mini-panels to NASA Lewis, we next fabricated a much larger fully functional panel comprising thirty-six total elements arranged in a six-by-six matrix, as shown in Figures 28 through 31. This panel was populated with Varian gallium arsenide cells. Each cell assembly included a cell, a prismatic cell cover, a copper heat spreader/back contact, and a copper wire/tab front contact (as discussed in Section 6.0). Prior to adhesively bonding them inside the panel, all the cell assemblies were first tested outdoors under the same mini-dome lens to determine the short-circuit current response of each cell. The cell assemblies were then grouped by short-circuit current into six groups of six cells each. Each group of current-matched cells was then bonded into a row within the prototype panel, and wired into a series circuit. Thus, the prototype panel consists of six independent circuits, each comprising six series-connected cells.

Next, all lenses were individually tested outdoors by allowing each lens to focus sunlight onto the same gallium arsenide cell assembly, while its short-circuit current was measured. Since the lenses were hand-made, using polycarbonate superstrates, this screening allowed us to reject poor performers, and to ensure that equally efficient lenses could be used in each six-cell series-connected circuit in the prototype panel.

The lenses were then aligned and bonded within the panel using an indoor collimated light source to simulate the sunlight. To allow one six-cell circuit to be observed and tested under one-sun conditions, we only permanently populated five of the six circuits with lenses. Thus, the prototype panel, as tested and delivered, had thirty total lenses. The panel was tested outdoors at ENTECH for performance, as further discussed below.

The cells used in the prototype panel were from a production run at Varian, and had lower efficiency levels than the earlier prototype Varian cells described in Section 5.1. In bare cell tests at NASA Lewis, these production cells were typically 19-20% efficient at 100 AMO suns and 25 degrees C, compared to about 22% for the prototype cells. Unfortunately, the NASA Lewis solar simulator facility was down for repairs during the panel development period, and prism-covered production cell efficiency levels could not be measured. Nevertheless, based on the previous tests on prototype prism-covered cells (discussed in Section 5.1), we estimate that the production cells should be 21-22% efficient after prism covering, at 100 AMO suns irradiance and 25 degrees

Figure 27 - Three-Element Mini-Panel and Key Components
(Photo Courtesy of Boeing)
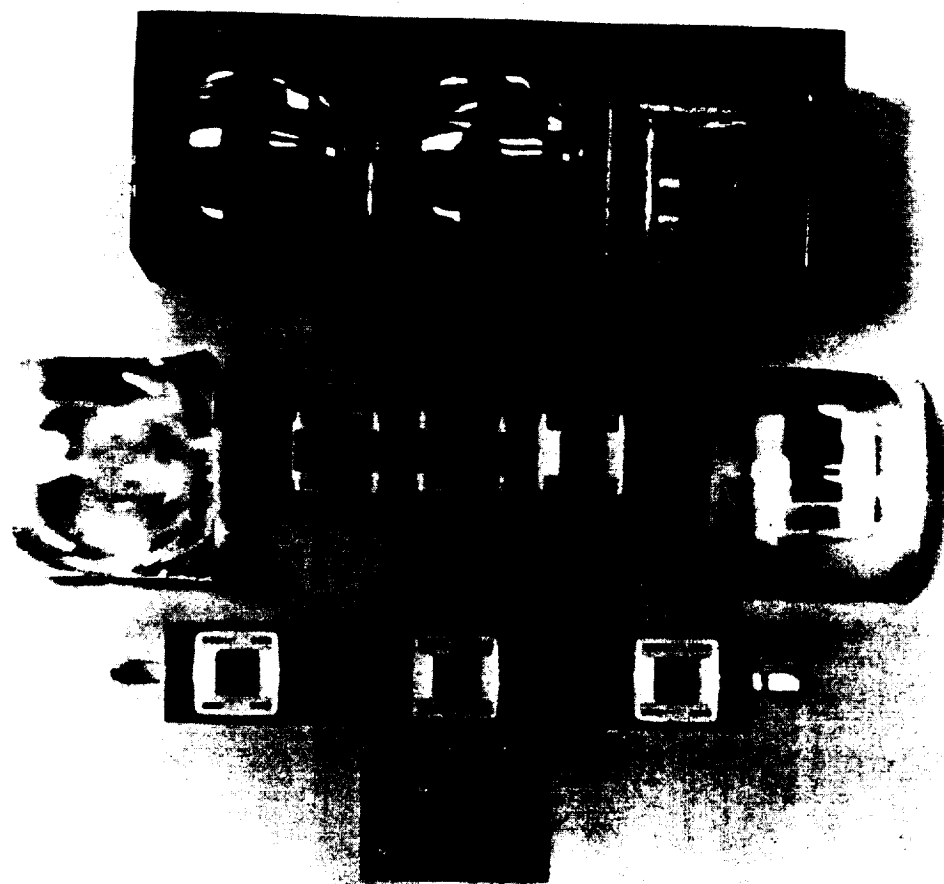
ENTECH, INC

Figure 28 - Thirty-Six Element Prototype Mini-Dome Lens
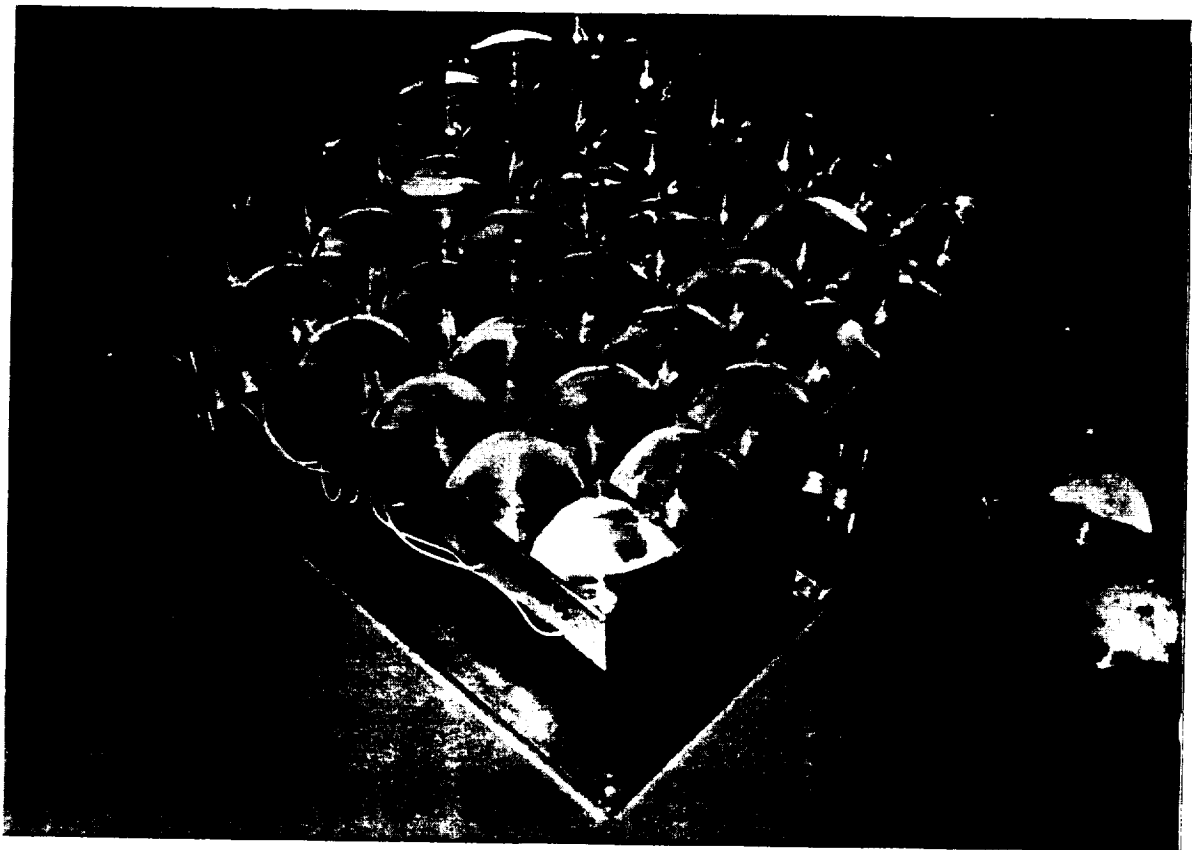Photovoltaic Concentrator Panel

ENTECH, INC.

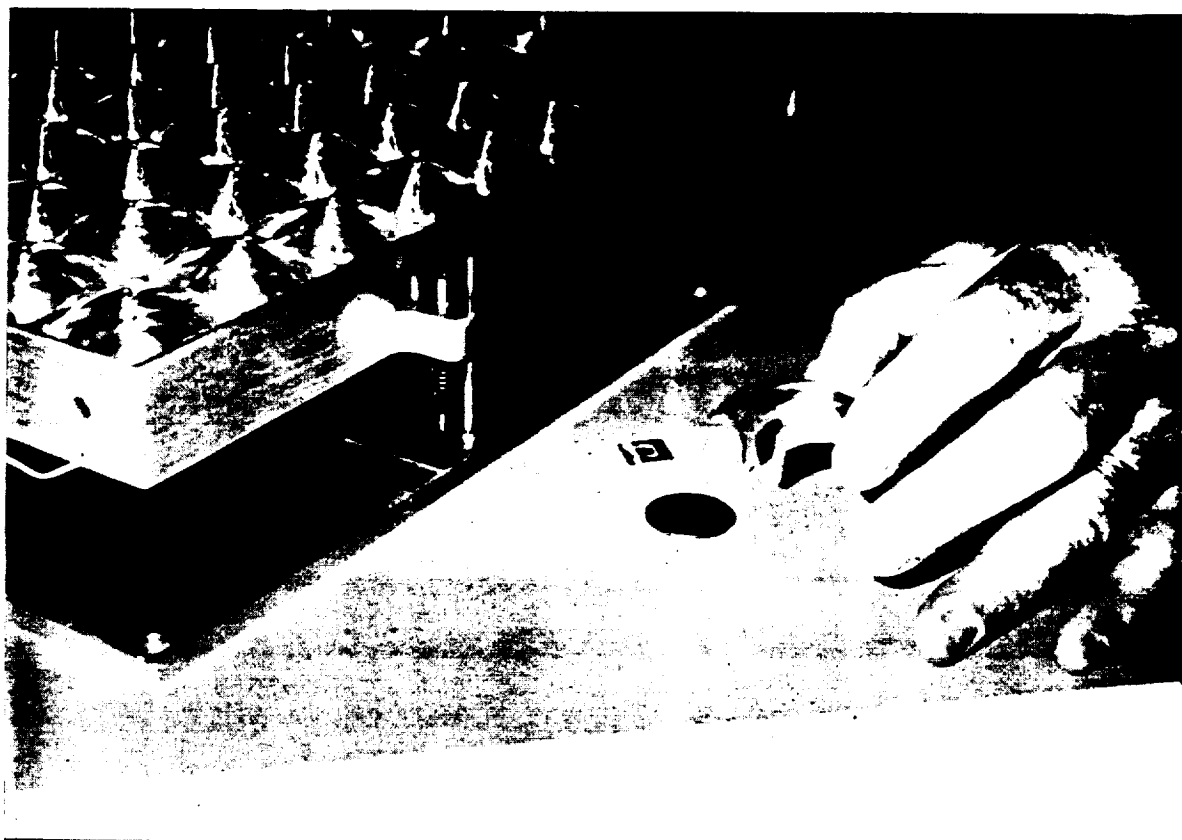Figure 29 - Components of the Prototype Panel

ENTECH, INC.

Figure 30 - Prototype Mini-Dome Lens Panel Under Outdoor Testing
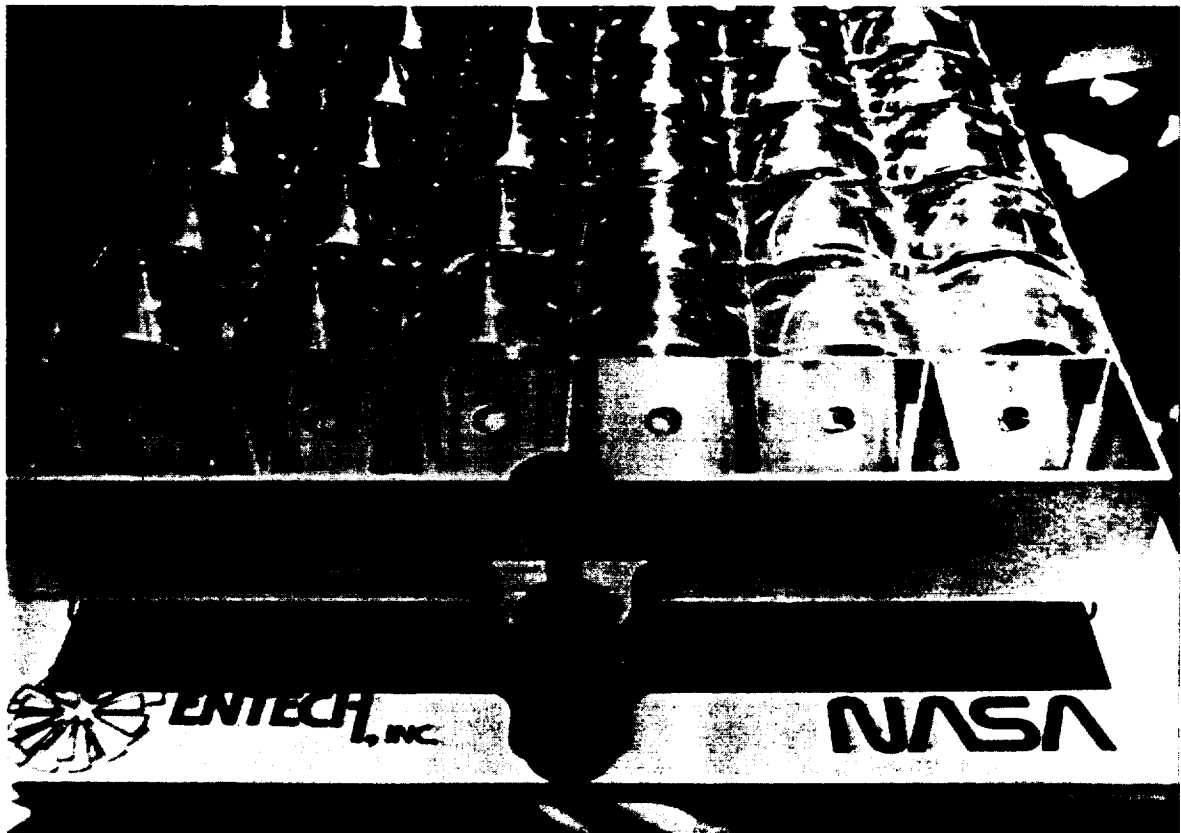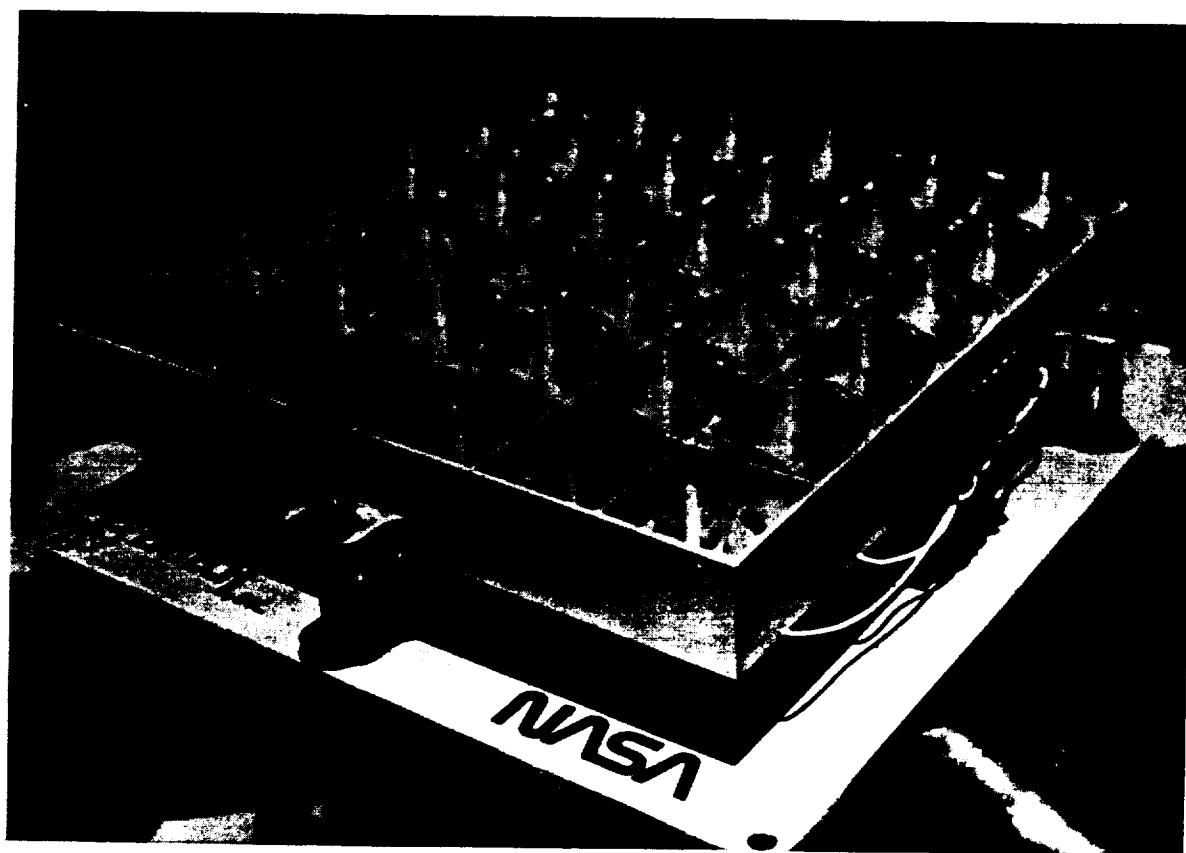

ENTECH, INC.

Figure 31 - Prototype Mini-Dome Lens Panel Under Outdoor Testing

C. Based on comparison tests performed on the same gallium arsenide cells by NASA Lewis under an AMO spectrum and by Sandia National Labs under an AM1.5D spectrum (the D corresponds to the direct normal portion of the solar spectrum which is focussed by a concentrator, as opposed to the global spectrum which includes the diffuse portion as well), we also estimate that these production cells should be 25-26% efficient at 100 AM1.5D suns irradiance and 25 degrees C (Reference 15). The higher terrestrial efficiency is due to the more beneficial match between the terrestrial solar spectrum and the gallium arsenide response spectrum, made possible by atmospheric filtering of the poorly converted ultraviolet and infrared portions of the solar spectrum. With 25-26% efficient cells, we would expect a lens/cell efficiency of about 22.5 - 23.5%, for a 90% efficient mini-dome lens. Indeed, we measured individual lens/cell elements at efficiency levels as high as 23.5% in outdoor tests. However, when six of the lens/cell elements are combined into a series-connected circuit, wiring and mismatch losses will reduce the circuit efficiency below the individual lens/cell efficiency levels. In conjunction with NASA Lewis personnel, we generally assume a factor of 93% to treat this wiring and mismatch loss. Using such a factor on the prototype panel reduces the expected terrestrial six-element circuit efficiency to about 22%. Indeed, in outdoor tests, we measured six-element circuit efficiency levels above 21%, as summarized in Figure 32. Thus, the measured prototype panel performance was close to expected values, based on the production cell efficiency levels.

The prototype panel has been delivered to NASA Lewis for further evaluation. We believe that this first prototype panel has demonstrated that the mini-dome lens panel approach is simple and practical to implement in functional hardware.

Figure 32 - Outdoor Test Results on the Six-by-Six Element Prototype Panel

Panel Description: Six cell strings of six series-connected cells each.

Five strings populated with dome lenses, one string bare.

Single lens aperture measured at 13.6 sq.cm.

Six-lens cell string aperture at 81.6 sq.cm.

Test Conditions: Ambient temperature: 25-30 degrees C.

Cell temperature: 45-51 degrees C.

Direct normal irradiance: 840-860 W./sq.m.

Location: Dallas-Fort Worth Airport, Texas.

Date: 6 August 1990.

Results:

String Number	String Efficiency (Corrected to 25C Cell Temp)
1	21.2%
2	21.1%
3	21.2%
4	20.5%
5	19.9%

ENTECH, INC.

## 9.0 Updated System Performance, Mass, and Specific Power Estimates

Based on the results of this Phase II SBIR program, as discussed in the previous sections, we have updated our estimates of system performance, mass, and specific power, as discussed in the following paragraphs.

Figure 33 summarizes the baseline NASA panel mass breakdown. For each panel element, the material, density, and thickness are specified. In addition, the element surface area to panel area ratio is shown. By combining the element density, thickness, and area ratio, the element's contribution to the panel's mass per unit area is determined. Note that the overall panel mass corresponds to about 2.4 kg/sq.m. of panel area. Note also that the microglass contributes about 20% of the total panel mass, while the aluminum radiator and honeycomb together contribute about 60% of the total panel mass. The glass mass can possibly be reduced either by making the glass thinner or by using a less dense, non-glass superstrate. The aluminum mass can undoubtedly be reduced by optimizing the honeycomb/radiator assembly, including lightening holes, gussets to support thinner walls, stiffeners along wall edges, tapered radiator sheets, etc., all of which are compatible with the computer-controlled milling production process described in Section 7.0.

Figure 34 indicates what may be possible in the future for an ultra-light version of the mini-dome lens panel. If the superstrate can be replaced by a coating or by a less dense material, the lens mass can be reduced accordingly. If the machined honeycomb/radiator structure can be optimized to approach the mass corresponding to 50 micron thick walls and floors, the aluminum mass can be reduced accordingly. With these changes, the mass per unit area of the panel should approach 1 kg/sq.m. We refer to this design as the SDIO lightweight panel.

To estimate the mass of a full space solar array (wing) based on the mini-dome lens panel approach, we need to add the mass of an automatically deploying support structure to the panel mass discussed above. As previously discussed in Section 2.0, such automatically deploying support structures are being developed by other organizations for use with heavier, less efficient, reflective photovoltaic concentrator panels. The mass contribution of these support structures is typically about 0.7 kg per square meter of panel supported, for relatively heavy reflective concentrator panels (i.e., 6 kg/sq.m. panel mass). Since the major structural forces in orbit are due to accelerations, these forces are proportional to panel mass. Since the mass of the mini-dome lens panels is much less than for the reflective concentrator panels, the loads on the underlying support structure will be much less. Therefore, the mass of the support structure should be much lower for use with the mini-dome lens panels than for use with reflective concentrator panels. Nevertheless, for our baseline NASA panel, we will assume that the support structure contributes 0.7 kg/sq.m. to the array mass. However, for our lightweight SDIO panel, we will assume that a six-fold decrease in panel mass (compared to reflective panels) will allow at least a 40% reduction in support structure mass, for a contribution of 0.4 kg/sq.m. These mass values will be included in the specific power estimates discussed below.

Figure 35 summarizes our updated estimates of panel performance and specific power, based on the current prototype lens and cell test results described in this report. The first column corresponds to a single-junction gallium arsenide (GaAs) cell in the NASA baseline panel. Previously predicted cell efficiency
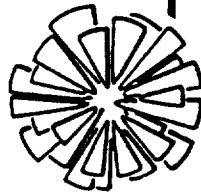
ENTECH, INC.

MINI-DOME LENS SPACE PHOTOVOLTAIC CONCENTRATOR
NASA BASELINE PANEL MASS BREAKDOWN

ELEMENT	MATERIAL	DENSITY (G/CU.CM.)	THICKNESS (CM)	SURFACE AREA / PANEL AREA	MASS/PANEL AREA (KG/SQ.M.)
LENS SUPERSTRATE	MICROGLASS	2.50	0.015	1.30	0.49
LENS PRISMS	SILICONE	1.00	0.015*	1.30	0.19
RADIATOR	ALUMINUM	2.77	0.020	1.00	0.55
CELL/COVER/MOUNT	GAAS ET AL	5.70	0.046	0.02	0.05
HONEYCOMB	ALUMINUM	2.77	0.015	2.20	0.91
RADIATOR COATING	ALUMINA	3.88	0.001	2.00	0.08
MISCELLANEOUS	-------- 7.5% OF ABOVE TOTAL --------				0.17
TOTAL					2.44

* SILICONE BASE THICKNESS = 0.010 CM
  SILICONE PRISM THICKNESS = 0.010 CM (BUT HALF VOID)
  EFFECTIVE SILICONE THICKNESS = 0.015 CM

Figure 33
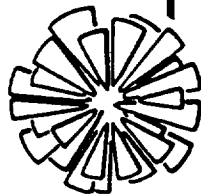
ENTECH, INC.

MINI-DOME LENS SPACE PHOTOVOLTAIC CONCENTRATOR
SDIO LIGHTWEIGHT PANEL MASS BREAKDOWN

ELEMENT	MATERIAL	DENSITY (G/CU.CM.)	THICKNESS (CM)	SURFACE AREA/PANEL AREA	MASS/PANEL AREA (KG/SQ.M.)
LENS SUPERSTRATE	SILICONE	1.00	0.015	1.30	0.19
LENS PRISMS	SILICONE	1.00	0.015*	1.30	0.19
RADIATOR	ALUMINUM	2.77	0.005	1.00	0.14
CELL/COVER/MOUNT	GAAS ET AL	5.70	0.046	0.02	0.05
HONEYCOMB	ALUMINUM	2.77	0.005	2.20	0.30
RADIATOR COATING	ALUMINA	3.88	0.001	2.00	0.08
MISCELLANEOUS	-------- 7.5% OF ABOVE TOTAL --------				0.07
TOTAL					1.02

```
* SILICONE BASE THICKNESS         = 0.010 CM
  SILICONE PRISM THICKNESS        = 0.010 CM (BUT HALF VOID)
  EFFECTIVE SILICONE THICKNESS    = 0.015 CM
```
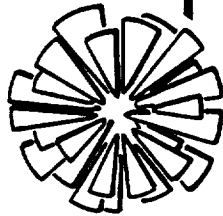
Figure 34

ENTECH, INC.

MINI-DOME FRESNEL LENS ARRAY - UPDATED PERFORMANCE ESTIMATES
BASED ON RECENT TEST RESULTS FOR PROTOTYPE CELLS AND LENSES

ITEM	BASELINE w/GAAS (NEAR-TERM)	BASELINE w/TANDEM (NEAR-TERM)	IMPROVED SDIO ULTRALIGHT (LONGER-TERM)
CELL TYPE	GAAS	GAAS + GASb	GAAS + GASb
CELL EFF. AT 25C	24%	24% + 7% = 31%	24% + 8% = 32%
CELL OPERATING TEMP.	100C	100C & 100C	130C & 130C
CELL EFF. AT OPER. TEMP.	22%	22% + 5% = 27%	21% + 5% = 26%
LENS EFFICIENCY	90%*	90%*	95%
PACKING FACTOR	97%	97%	97%
MISMATCH/WIRING FACTOR	93%	93%	93%
ARRAY EFFICIENCY	18%	22%	22%
POWER DENSITY (W/SQ.M.)	247	302	302
PANEL MASS (KG/SQ.M.)	2.4	2.4	1.0
STRUCTURE MASS (KG/SQ.M.)	0.7	0.7	0.4
ARRAY MASS (KG/SQ.M.)	3.1	3.1	1.4
SPECIFIC POWER (W/KG)	80	97	216

NOTES: 1. UNDERLINING DENOTES MEASURED PERFORMANCE PARAMETERS FOR PROTOTYPE CELLS AND LENSES.

2. ASTERISK (*) DENOTES LENS WITHOUT ANTIREFLECTION COATINGS.

FIGURE 35

levels of 24% at room temperature and 22% at operating temperature have now been confirmed by NASA Lewis. Similarly, the 90% mini-dome lens net optical efficiency has also been confirmed by NASA Lewis. Including a 97% aperture-to-panel packing factor and a 93% wiring/mismatch factor, the expected array efficiency is 18%, corresponding to an areal power density of 245 W/sq.m. With a 3.1 kg/sq.m. array mass (including panel and support structure), the specific power should be 79 W/kg for this GaAs-based array.

The second column of Figure 35 corresponds to a simple substitution of the Boeing tandem gallium cell for the gallium arsenide cell in the NASA baseline panel. NASA has confirmed a 7% boost efficiency for the GaAs-filtered gallium antimonide (GaSb) back cell, bringing the total tandem cell efficiency to 31%. While the operating temperature should be less for the more efficiency tandem cell (due to a lower waste heat load), we have used the same 100 degree C operating temperature estimate in Figure 35 to arrive at an operational tandem cell efficiency of 27%. When combined with lens efficiency, packing factor, and wiring/mismatch factor, the tandem cell baseline array should provide an efficiency of 22% and corresponding areal power density of 300 W/sq.m. At the same 3.1 kg/sq.m. array mass, the new tandem cell array should approach 100 W/kg in specific power.

The third column of Figure 35 corresponds to a longer-term, ultra-light array using the tandem gallium cells. The tandem cell efficiency at room temperature will undoubtedly improve with further development and refinement of the new GaSb back cell. A value of 32% is included in the longer-term column of Figure 35 to reflect such improvements. However, the ultralight panel will involve higher operating cell temperatures (as discussed in Section 7.0), with a corresponding reduction in cell operating efficiency. Assuming a 130 degree C operating point, the tandem cell efficiency should be about 26%. Antireflection coatings on the lens surfaces should increase lens optical efficiency from the current 90% value to about 95% in the longer term. Including packing factor and wiring/mismatch losses, the longer-term array should maintain the 22% efficiency and the 300 W/sq.m. areal power density. However, with its much lower array mass of 1.4 kg/sq.m., the longer-term array appears capable of a specific power level above 200 W/kg.

Since the data summarized in Figure 35 represent a straightforward scorecard for the mini-dome lens array technology, NASA and ENTECH continually update these data based on the latest analytical and experimental developments. The updated values are then published in periodic technical papers presented at IEEE, IECEC, and SPRAT conferences (e.g., References 16 through 20).

To summarize the results discussed above, we now believe that the mini-dome lens space photovoltaic concentrator array is capable of reaching an areal power density of 300 W/sq.m. in the near term. In addition, the new array is capable of reaching a specific power of 100 W/kg in the near term, and about twice that value in the longer term.

10.0 Conclusions

The primary conclusion drawn from this Phase II SBIR program is that the unprecedented performance levels predicted in Phase I for the mini-dome lens concentrator array have now been confirmed. Supporting conclusions include the following:

1. The new mini-dome lens has a NASA-measured net optical efficiency of 90% at 109X geometrical concentration under AMO irradiance, with no antireflection coatings on the lens.

2. The new mini-dome lens has a measured sun-pointing error tolerance of 1 degree, with less than a 1% degradation in optical efficiency at this design pointing error condition.

3. Prototype mini-dome lenses have been successfully made in three structures to date: (i) monolithic silicone rubber lens; (ii) silicone rubber lens bonded to polycarbonate superstrate; and (iii) silicone rubber lens bonded to microglass superstrate.

4. The prismatic cell cover provides essentially complete elimination of the gridline obscuation loss normally encountered in photovoltaic cells, based on NASA measurements of cell performance before and after prismatic cover application.

5. Single-junction gallium arsenide (GaAs) cells (made by both Varian and Boeing) with prism covers have achieved 24% efficiency at 25 degrees C and 22% efficiency at 100 degrees C, in simulator tests by NASA Lewis at 100 AMO suns irradiance.

6. Gallium arsenide-filtered gallium antimonide (GaSb) infrared booster cells (made by Boeing) with prism covers have achieved a 7% boost efficiency at 25 degrees C and 100 AMO suns irradiance, in tests by NASA Lewis.

7. Tandem GaAs/GaSb cells (made by Boeing) with prism covers on both cells have achieved 31% combined efficiency at 25 degrees C and 100 AMO suns irradiance, in tests by NASA Lewis.

8. A simple, rapid, cost-effective approach for machining the honeycomb/radiator assembly from a thick plate of aluminum has been selected and verified in hardware, as demonstrated by a thirty-six element panel.

9. Practical near-term goals for the mini-dome lens photovoltaic concentrator array have been upwardly revised to 300 W/sq.m. in terms of areal power density and 100 W/kg in terms of specific power.

The key features and advantages of the mini-dome lens space photovoltaic concentrator system are summarized in Figure 36.
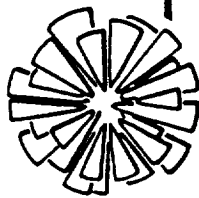
ENTECH, INC.

MINI-DOME LENS SPACE PHOTOVOLTAIC CONCENTRATOR
KEY FEATURES AND ADVANTAGES

UNIQUE LENS: THE TRANSMITTANCE-OPTIMIZED DOME LENS PROVIDES 90% NET OPTICAL EFFICIENCY (WITHOUT THE NEED FOR SECONDARY OR TERTIARY CONCENTRATORS), EXCEPTIONAL TOLERANCES FOR MANUFACTURING AND OPERATIONAL INACCURACIES (E.G., 200 TIMES THE SLOPE ERROR TOLERANCE OF REFLECTIVE CONCENTRATORS, AND 100 TIMES THE SLOPE ERROR TOLERANCE OF FLAT FRESNEL LENSES), AND EXCELLENT AND SELECTABLE TRACKING ERROR TOLERANCE (1 DEGREE FOR 4 MM CELL, 2 DEGREES FOR 5.4 MM CELL, ETC.)

CELL USAGE: VARIOUS CELLS CAN BE USED IN THE DOME LENS CONCENTRATOR, INCLUDING BOEING'S GAAS/GASB, VARIAN'S GAAS, NASA's INP, ET AL. (DUE TO HIGH CONCENTRATION, ONLY 1% OF NORMAL CELL AREA IS NEEDED).

PRISMATIC COVERS: ALLOW HEAVY GRID COVERAGE FOR EFFICIENT CURRENT COLLECTION.

HEAT REJECTION: CELLS ARE MOUNTED DIRECTLY TO A BACKSIDE RADIATOR.

PACKING FACTOR: LENSES CAN BE CUT SQUARE (OR HEX) IN APERTURE TO MAXIMIZE LENS APERTURE/PANEL AREA RATIO (97% IS EASILY ACHIEVED).

MODULARITY: THE NUMBER OF LENS/CELL ELEMENTS CAN BE SELECTED FOR OPTIMAL PANEL OUTPUT.

MATERIALS: READILY AVAILABLE LIGHTWEIGHT MATERIALS ARE USED THROUGHOUT THE PANEL.

MANUFACTURABILITY: ALL PANEL ELEMENTS APPEAR TO BE READILY MANUFACTURABLE.

DEPLOYABILITY: AUTOMATICALLY DEPLOYING STRUCTURES BEING DEVELOPED FOR OTHER CONCENTRATORS CAN BE EASILY ADAPTED TO THE MINI-DOME PANELS. (E.G., THE ASTRO-AEROSPACE ESS OR STACBEAM STRUCTURES).

Figure 36

- 54 -

11.0 Recommendations for Future Work

Based on the promising program results to date (documented in the preceeding ten sections of this report), we strongly recommend that NASA accelerate the development of the mini-dome lens space photovoltaic concentrator system. Since the mini-dome lens array offers more than double the areal power output of state-of-the-art planar silicon arrays, at equivalent or lower areal mass, this new space power technology could provide decisive advantages for major space missions planned for the next decade by NASA and DOD. Several specific technical areas, which could result in significant system improvement with future work, are briefly summarized below.

1. Development work toward a monolithic lens should continue. Polymeric lens materials with protective coatings (against ultraviolet radiation and/or monatomic oxygen) need further investigation. Cast sol-gel glass lens materials likewise need further evaluation.

2. Development work toward an all-glass prismatic cell cover should be initiated. Glass is, of course, one of the most stable, durable materials available. Furthermore, it provides excellent protection for solar cells against particulate radiation (electrons and protons) damage. Additionally, it can tolerate exposure to much higher temperatures than other prism cover materials, and it is amenable to electrostatic bonding.

3. Development of the next generation radiator/honeycomb structure should begin now. Alternate materials (e.g., carbon graphite, magnesium, etc.) should be investigated, as well as alternate configurations (e.g., hexagonal honeycomb, tapered backplane radiators, etc.). Structural analyses of the leading candidate designs should be conducted.

4. Thermal analysis and design activities should be expanded. Conceptual design and trade studies should be conducted for various panel configurations, using different thermal control coatings, for systems operating in orbits ranging from LEO to GEO.

5. Environmental testing of key candidate system components should begin, including thermal cycling, radiation exposure, vibration testing, etc.

6. Analysis, design and development of an automatically deployable support structure specifically tailored for the mini-dome lens panels should begin. Previous support structure approaches for reflective concentrating photovoltaic systems are over-designed for the mini-dome lens panels. Simpler, lighter structures should be developed for the new panels.

12.0 References

1. M.J. O'Neill et al, "Development of a Fresnel Lens Gallium Arsenide Photovoltaic Concentrator for Space Applications," Phase I Final Report, NASA SBIR Contract No. NAS3-24871, ENTECH, Inc., DFW Airport, 1986.

2. M.J. O'Neill, "Solar Concentrator and Energy Collection System," U.S. Patent No. 4,069,812, 1978.

3. M.J. O'Neill, "A Unique New Fresnel Lens Solar Concentrator," ISES, Atlanta, 1979.

4. M.J. O'Neill and R.A. Waller, "Analytical/Experimental Study of the Optical Performance of a Transmittance-Optimized Linear Fresnel Lens Solar Concentrator," ISES, Phoenix, 1980.

5. M.J. O'Neill, "Five-Year Performance Results for the Dallas-Fort Worth (DFW) Airport Solar Total Energy System," ASHRAE Transactions, Vol. 94, Part 1, 1988.

6. M.J. O'Neill et al, "Development, Deployment, and Startup of the 2,000 Sq.M. Linear Fresnel Lens Photovoltaic Concentrator System at 3M/Austin (Texas)," ASES Solar 90, Austin, 1990.

7. M.J. O'Neill et al, "Fabrication, Installation, and Initial Operation of the 2,000 sq.m. Linear Fresnel Lens Photovoltaic Concentrator System at 3M/Austin (Texas)," 21st IEEE PVSC, Orlando, 1990.

8. M.J. O'Neill, "Photovoltaic Cell Cover for Use with a Primary Optical Concentrator in a Solar Energy Collector," U.S. Patent No. 4,711,972, 1987.

9. M.J. O'Neill, "Two Linear Fresnel Lens Photovoltaic Concentrator Design Innovations: A Prismatic Cell Cover and a Copper Heat Spreader," U.S. Department of Energy Report No. DOE/ER/80126-1, 1985.

10. M.J. O'Neill, "Measured Performance of a 22.5X Linear Fresnel Lens Solar Concentrator Using Prismatically Covered Polycrystalline Silicon Cells," 19th IEEE-PVSC, New Orleans, 1987.

11. M. Mobrem, "High-Performance Deployable Structures for the Support of High-Concentration Ratio Solar Array Modules," Final Report, NASA Contract No. NAS8-36043, Astro Aerospace Corporation, Carpinteria, CA, 1985.

12. M.F. Piszczor et al, "High Altitude AMO Testing of PV Concentrator Lens Elements," 21st IEEE-PVSC, Orlando, 1990.

13. L.M. Fraas et al, "Tandem Solar Cells with 31% (AMO) and 37% (AM1.5D) Energy Conversion Efficiencies," IEEE AES Magazine, November 1989.

14. J.E. Avery et al, "Ligthweight Concentrator Module with 30% AMO Efficient GaAs/GaSb Tandem Cells," 21st IEEE PVSC, Orlando, 1990.

15. M.J. O'Neill and M.F. Piszczor, "An Advanced Space Photovoltaic Concentrator Array Using Fresnel Lenses, Gallium Arsenide Cells, and Prismatic Cell Covers," 20th IEEE PVSC, Las Vegas, 1988.

16. M.F. Piszczor, C.K. Swartz, et al, "The Mini-Dome Fresnel Lens Photovoltaic Concentrator Array: Current Status of Component and Prototype Panel Testing," 21st IEEE PVSC, Orlando, 1990.

17. M.F. Piszczor and M.J. O'Neill, "Development of an Advanced Concentrator System for Space Applications," 22nd IECEC, Philadelphia, 1987.

18. M.F. Piszczor and M.J. O'Neill, "Domed Fresnel Lens Concentrator Technology for Space Application," 9th NASA SPRAT Conference, Cleveland, 1988.

19. M.J. O'Neill and M.F. Piszczor, "Mini-Dome Fresnel Lens Photovoltaic Concentrator Development," 10th NASA SPRAT Converence, Cleveland, 1989.

20. M.F. Piszczor, C.K. Swartz, et al, "Component and Prototype Panel Testing of the Mini-Dome Fresnel Lens Photovoltaic Concentrator Array," 25th IECEC, Reno, 1990.